

# 1 Analysis of the potential of near ground measurements of 2 CO<sub>2</sub> and CH<sub>4</sub> in London, UK for the monitoring of city-scale 3 emissions using an atmospheric transport model.

4  
5 A. Boon<sup>1</sup>, G. Broquet<sup>2</sup>, D. J. Clifford<sup>1</sup>, F. Chevallier<sup>2</sup>, D. M. Butterfield<sup>3</sup>, I. Pison<sup>2</sup>,  
6 M. Ramonet<sup>2</sup>, J.D. Paris<sup>2</sup> and P. Ciais<sup>2</sup>.

7  
8 [1] Department of Meteorology, University of Reading, Reading, Berkshire RG6 6BB, UK

9 [2] Laboratoire des Sciences du Climat et de l'Environnement, CEA-CNRS-UVSQ,  
10 UMR8212, IPSL, Gif-sur-Yvette, France

11 [3] National Physical Laboratory, Teddington, Middlesex, TW11 0LW, UK

12 Correspondence to: A. Boon (alex.boon@reading.ac.uk)

## 13 14 **Abstract**

15 Carbon dioxide (CO<sub>2</sub>) and methane (CH<sub>4</sub>) mole fractions were measured at four near ground  
16 sites located in and around London during the summer of 2012 in view to investigate the  
17 potential of assimilating such measurements in an atmospheric inversion system for the  
18 monitoring of the CO<sub>2</sub> and CH<sub>4</sub> emissions in the London area. These data were analysed and  
19 compared with simulations using a modelling framework suited to building an inversion  
20 system: a 2-km horizontal resolution South of England configuration of the transport model  
21 CHIMERE driven by European Centre for Medium-Range Weather Forecasts (ECMWF)  
22 meteorological forcing, coupled to a 1-km horizontal resolution emission inventory (the UK  
23 National Atmospheric Emission Inventory). First comparisons reveal that local sources, that  
24 cannot be represented in the model at a 2-km resolution, have a large impact on  
25 measurements. We evaluate methods to minimise some of the other critical sources of  
26 discrepancies between the measurements and the model simulation that overlap with the  
27 impact of the errors in the emission inventory. These methods should make it easier to  
28 identify the corrections that should be applied to the inventory. Analysis is supported by  
29 observations from meteorological sites around the city and a three-week period of

1 atmospheric mixing layer height estimations from lidar measurements. The difficulties of  
2 modelling the mixing layer depth and thus CO<sub>2</sub> and CH<sub>4</sub> concentrations during the night,  
3 morning and late afternoon lead to focus on the afternoon period for all further analyses. The  
4 discrepancies between observations and model simulations are high for both CO<sub>2</sub> and CH<sub>4</sub>  
5 (i.e., their root mean square (RMS) is between 8 and 12 parts per million (ppm) for CO<sub>2</sub> and  
6 between 30 and 55 parts per billion (ppb) for CH<sub>4</sub> at a given site). By analysing the gradients  
7 between the urban sites and a suburban or rural reference site, we are able to decrease the  
8 impact of uncertainties in the fluxes and transport outside the London area and in the model  
9 domain boundary conditions. We are thus able to better focus attention on the signature of  
10 London urban CO<sub>2</sub> and CH<sub>4</sub> emissions in the atmospheric CO<sub>2</sub> and CH<sub>4</sub> concentrations. This  
11 considerably improves the statistical agreement between the model and observations for CO<sub>2</sub>  
12 (with model–data RMS discrepancies that are between 3 and 7 ppm) and to a lesser degree for  
13 CH<sub>4</sub> (with model–data RMS discrepancies that are between 29 and 38 ppb). Between one of  
14 the urban sites and either reference site, selecting the gradients during periods wherein the  
15 reference site is upwind of the urban site further decreases the statistics of the discrepancies in  
16 general even though not systematically. In a final attempt to focus on the signature of the city  
17 anthropogenic emission in the mole fraction measurements, we use a theoretical ratio of  
18 gradients of carbon monoxide (CO) to gradients of CO<sub>2</sub> from fossil fuel emissions in the  
19 London area to diagnose observation based fossil fuel CO<sub>2</sub> gradients, and compare them with  
20 the modelled ones. This estimate increases the consistency between the model and the  
21 measurements when considering one of the urban sites, but not when considering the other.  
22 While this study evaluates and highlights the asset of different approaches for increasing the  
23 consistency between the mesoscale model and the near ground data, and while it manages to  
24 decrease the random component of the analysed model–data discrepancies to an extent that  
25 should not be prohibitive to extracting the signal from the London urban emissions, large  
26 biases remain in the final model–data discrepancies. Such biases are likely related to local  
27 emissions to which the urban near ground sites are highly sensitive. This questions our current  
28 ability to exploit urban near ground data for the atmospheric inversion of city emissions based  
29 on models at spatial resolution coarser than 2-km. Several measurement and modelling  
30 concepts are discussed to overcome this challenge.

31

## 1 **1 Introduction**

2 As major emitters, cities have an important part to play in national greenhouse gas (GHG)  
3 emission reporting. Over half of the world's population now live in cities, and the UN  
4 estimate that the urban population will almost double from 3.4 to 6.3 billion by 2050 (United  
5 Nations, 2012). In the face of this continued urban population increase, cities can expect  
6 increased anthropogenic emissions unless measures are taken to reduce the impact of city life  
7 on the atmosphere. The majority of anthropogenic carbon dioxide (CO<sub>2</sub>) is released in the  
8 combustion of fossil fuels for heating, electricity and transport, the latter of which is  
9 particularly important in the urban environment. The major sources of methane (CH<sub>4</sub>) in city  
10 environments are leakage from natural gas infrastructure, landfill sites, wastewater treatment  
11 and transport emissions (Lowry et al., 2001; Nakagawa et al., 2005; Townsend-Small et al.,  
12 2012).

13 International agreements to limit GHG emissions make use of countries' self-reporting of  
14 emissions using emission inventories. These inventories are based upon activity data and  
15 corresponding emission factors and uncertainties can be substantial, particularly at the city  
16 scale. Ciais et al. (2010a) showed uncertainties of 19% of the mean emissions at country scale  
17 in the 25 EU Member States and up to 60% at scales less than 200-km. Currently there is no  
18 legal obligation for individual cities to report their emissions; however, as environmental  
19 awareness increases and actions are taken to reduce urban emissions, monitoring of city  
20 emissions to evaluate the success of emissions reduction schemes becomes an important  
21 consideration.

22 Quantifying GHG emissions from cities using an atmospheric inversion approach (i.e., based  
23 on gas mole fraction measurements, atmospheric transport modelling and statistical  
24 inference), is a relatively new scientific endeavour (Levin et al., 2011; McKain et al.,  
25 2012; Kort et al., 2013; Bréon et al., 2015; Henne et al., 2016; Stauffer et al., 2016).  
26 Instrumentation has been placed on tall masts or towers (at more than 50 m above the ground  
27 level, magl) or at near ground (at less than 20 magl) heights (Bréon et al., 2015; Lac et al.,  
28 2013; McKain et al., 2012) with a preference generally given to higher level measurement  
29 sites as these are expected to reduce variability due to local sources (Ciais et al., 2010b). The  
30 city-scale inversion studies have mainly focused on the monitoring of CO<sub>2</sub> city emissions.  
31 However, (McKain et al., 2015) have shown the potential of the approach to reduce

1 uncertainties in CH<sub>4</sub> city emissions inventories, which can be substantial in cities where the  
2 gas distribution network has a high leakage level.

3 Near ground sites are cheaper and easier to install and maintain than tall towers. There are far  
4 more choices of location for the placing of instrumentation near ground than on tall towers,  
5 even within a city. The development of cheaper instruments could enable the deployment of  
6 networks with numerous sites and this is likely to require placement of at least some sites on  
7 near ground locations. If near ground sites can be used effectively they could be highly  
8 complementary to the developing GHG observation networks. Bréon et al. (2015) and Stauffer  
9 et al. (2016) used near ground measurements taken in the suburban area of Paris but not in the  
10 city centre. They indicated that the capability of exploiting urban measurements would  
11 strongly improve the monitoring of the city emissions. Kort et al. (2013) evaluated (through  
12 Observing System Simulation Experiments, which is a common practice in the data  
13 assimilation community, as detailed by Masutani (2010)) different configurations of surface  
14 station networks for monitoring emissions from Los Angeles, and concluded that robust  
15 monitoring of megacities requires multiple in-city surface sites (numbering at least eight  
16 stations for Los Angeles). McKain et al. (2012) employed near ground sites in Salt Lake City,  
17 an urban area that is relatively small and topographically confined. They concluded that  
18 surface stations could be used to detect changes in emissions at the monthly scale, but not to  
19 derive estimates of the absolute emissions because of the inability of current models to  
20 simulate small scale atmospheric processes.

21 Our study feeds such an investigation of the potential of city atmospheric inversion  
22 frameworks using continuous measurements at near ground stations, including measurements  
23 within the urban area. We focus our attention on the megacity of London, UK. Previous  
24 studies of the GHG fluxes in London by the atmospheric community have largely focused on  
25 direct measurements of local fluxes using the eddy covariance technique, and on high  
26 resolution transport modelling to identify the emission (spatial) footprint associated with these  
27 measurements (Helfter et al., 2011;Kotthaus and Grimmond, 2012;Ward et al., 2015). These  
28 local eddy covariance measurements in London have been used to derive estimates of the  
29 fluxes for specific boroughs or administrative areas (Helfter et al., 2011) and to compare the  
30 typical fluxes for different types of land use (Ward et al., 2015).

31 The atmospheric inversion approach, which is based on different estimation concepts and  
32 modelling scales, has the potential to provide estimates of the emissions for a far larger

1 portion of the city, and ideally for the city as a whole. Rigby et al. (2008) compared CO<sub>2</sub>  
2 concentration measurements from a central London site (Queen's Tower, Imperial College)  
3 with near ground measurements at a more rural location (Royal Holloway University of  
4 London) upstream of the city in the prevailing wind direction. They thus characterised the  
5 CO<sub>2</sub> mole fraction enhancement as a result of the CO<sub>2</sub> emissions from anthropogenic sources  
6 in the city. Hernandez-Paniagua et al. (2015) recently analysed the long-term time series at  
7 the Royal Holloway site to study the long-term trends and seasonal variation in CO<sub>2</sub> mole  
8 fractions, which are driven by the variations of the biological uptake and of the anthropogenic  
9 activities underlying the city emissions. However, to our knowledge, these data have not yet  
10 been exploited using the inversion approach to quantify the city emissions. More recently,  
11 O'Shea et al. (2014) and Font et al. (2015) took airborne measurements of CO<sub>2</sub> mole fractions  
12 over London and combined these with box models to estimate vertical fluxes and a  
13 Lagrangian particle model to estimate the area ("footprints") corresponding to these fluxes.  
14 O'Shea et al. (2014) compared the flux estimates with eddy covariance flux measurements and  
15 the estimate of the city emissions from the 2009 UK National Atmospheric Emissions  
16 Inventory (NAEI) (NAEI, 2013). In the course of their analysis, Font et al. (2015) indicated  
17 that the uncertainties associated with footprint modelling are high and that there is a need to  
18 improve their protocol to separate the natural and anthropogenic CO<sub>2</sub> fluxes in their estimates,  
19 which is a traditional source of concern for the monitoring of anthropogenic emissions of CO<sub>2</sub>  
20 (Bréon et al., 2015). Regular aircraft campaigns could provide a good sampling of transitory  
21 city emissions but the continuous monitoring of these emissions would likely have to rely on  
22 continuous measurements from ground-based stations. The monitoring of CH<sub>4</sub> emissions or  
23 mole fractions in London remains limited (Lowry et al., 2001).

24 In this context, we made quasi-continuous measurements of CO<sub>2</sub>, CH<sub>4</sub> and CO during 2012 at  
25 four sites in the London area (two inner city sites, one suburban site and one rural site outside  
26 the urban area) using sensors located at 10–15 m above ground level. We assess the ability of  
27 a km-resolution transport model driven by a km-resolution emissions inventory to simulate  
28 these CO<sub>2</sub> and CH<sub>4</sub> measurements. The aim is to understand whether such measurement sites  
29 are ultimately suitable for use in a flux inversion scheme based on the km-resolution model.  
30 This study investigates the weight of different sources of discrepancies between observed and  
31 simulated GHG mole fractions (henceforth 'model–data discrepancies'). By decomposing the  
32 discrepancies depending on their different sources, we attempt to isolate and exploit the part  
33 of the discrepancies that are due to the errors in the estimates of the urban emissions. We

1 focus on the following sources of uncertainties and limitations when simulating the CO<sub>2</sub> and  
2 CH<sub>4</sub> measurements in the London area with the model, which we can assume to be significant  
3 sources of model–data discrepancies along with the errors in the estimate of the urban  
4 emissions:

5 (1) The differences of representativity in terms of spatial scale between the model and the  
6 measurements: near ground sites could be highly sensitive to very local emissions, i.e., at  
7 scales smaller than those represented by the model.

8 (2) Uncertainties in the modelled meteorological conditions, in particular in the wind speed  
9 and direction and in the mixing layer height above the city.

10 (3) Uncertainties relating to both the conditions at the model domain boundaries and to the  
11 modelling of the fluxes outside of the London area, which can influence the  
12 concentrations in the London area.

13 (4) In the case of CO<sub>2</sub>, uncertainties related to remote or near-field natural fluxes.

14 We introduce the measurement sites and model configuration in Sect. 2. In Sect. 3 we first  
15 consider issues of spatial representativity (Sect. 3.1) and then the ability of the model to  
16 simulate the diurnal cycle of mixing layer height, CO<sub>2</sub> and CH<sub>4</sub> (Sect 3.2). In Sect. 3.3 we  
17 compare winds simulated by the model to measurements at two surface meteorological  
18 stations. In Sect. 3.4 we examine the day-to-day variations of measured and modelled CO<sub>2</sub>  
19 and CH<sub>4</sub>. We attempt to remove the influence of the remote fluxes and conditions by  
20 considering gradients in CO<sub>2</sub> and CH<sub>4</sub> across the city in Sect. 3.5, and then take the wind  
21 direction into account when selecting the gradients (Sect. 3.6). Finally, we evaluate the  
22 modelled fossil-fuel CO<sub>2</sub> using a simple method to estimate the anthropogenic component of  
23 the observed CO<sub>2</sub> mole fractions based on the simultaneous CO observations (Sect. 3.7). A  
24 summary and discussion of the overall findings of the research is then given in Sect. 4.

25

## 26 **2 Methodology**

### 27 **2.1 London emissions inventory for CO<sub>2</sub> and CH<sub>4</sub>**

28 As context for the location of the in situ measurements, and to provide an estimate of the  
29 emissions applied within the model, we utilise the UK NAEI (NAEI, 2013), including a  
30 mapping of CH<sub>4</sub> sources from Dragosits and Sutton (2011). The NAEI provides annual  
31 gridded emission data for a wide range of atmospheric pollutants and GHGs with a sectorial

1 distribution by the main types of emitting activities: agricultural soil losses, domestic  
2 (commercial, residential, institutional) combustion, energy production, industrial combustion,  
3 industrial production processes, offshore own gas combustion, road transport, other transport,  
4 solvent use, waste treatment and disposal and (for CH<sub>4</sub> only) agricultural emissions due to  
5 livestock and natural emissions. Major CO<sub>2</sub> and CH<sub>4</sub> point sources (comprising large power  
6 and combustion plants) are also listed and localised individually. Significant sources of all  
7 these sectors apart from the offshore own gas combustion occur in the London urban area or  
8 in its immediate vicinity. The methodology applied to derive these gridded maps is described  
9 in Bush et al. (2010) and Dragosits and Sutton (2011).

10 The most up-to-date published emissions estimates available from NAEI at the time of this  
11 study were for 2009. The CO<sub>2</sub> emissions for the region around London are shown at 2-km  
12 resolution (the resolution of simulated transport; see Sect. 2.4) in Fig. 1 along with the  
13 position of the measurement stations (Sect. 2.2). In the vicinity of London, nearly all point  
14 sources of CO<sub>2</sub> are related to combustion processes with emissions from high stacks and  
15 through warm plumes. The 10 largest emitters in the domain defined by Fig. 1 are power  
16 stations, which represent nearly 27% of the emissions in this domain.

## 17 **2.2 GHG measurement site locations and characteristics**

18 The four measurement sites were located in and around London to sample air masses passing  
19 over London at various levels of sensitivity to urban emissions (in the city centre, suburban  
20 and rural areas). Note that no formal quantitative network design was applied beforehand to  
21 select the optimal location of the stations for their ability to constrain the emissions of  
22 London. The station locations were rather chosen based on the configuration of the emissions  
23 given by the inventory maps and the availability of suitable locations for installation and  
24 maintenance of the instruments.

25 The site locations are shown in Fig. 1 and were operational between June and September,  
26 2012. The two urban sites of Hackney and Poplar were located in central London, 6 km apart  
27 from each other and to the north-east of the main area of emissions (Hackney at 51° 33'  
28 31.45", -0° 3' 25.44"; Poplar 51° 30' 35.67", -0° 1' 11.33"). The suburban site was located in  
29 Teddington (51° 25' 13.63", -0° 20' 21.15), 17 km south-west of Central London. The  
30 location of this site was chosen a priori to allow the analysis of the gradient due to the city  
31 emissions when the wind blows from the south-west. This is usually the case and 52% of the

1 wind directions measured at Heathrow Airport (see Sect. 2.5) during the period July–  
2 September 2012 (i.e., our study period) were from the south-west sector. The fourth site was  
3 located in Detling, Kent ( $51^{\circ} 18' 28.44''$ ,  $0^{\circ} 34' 57.36''$ ), in a rural area approximately 50 km  
4 from the inner city and was selected to help to detect the influence of remote fluxes on the  
5 GHG mole fractions over the city.

6 The measurement stations at Hackney and Poplar were located on the rooftop of a college and  
7 a primary education school, respectively. The inlets for each of these sensors were placed  
8 approximately 10 m above street level and approximately 2 m above the rooftop level. The  
9 NAEI emissions map (Fig. 1) shows substantial CO<sub>2</sub> sources west of the Poplar and Hackney  
10 sites, relating to the city centre.

11 The site in Teddington was located on top of a building approximately 15 m from ground  
12 level. Teddington is referred to in this study as a suburban site, due to its location in a  
13 residential area beside Bushy Park. Bushy Park represents a large area of vegetation cover  
14 surrounding the site to the east, south and west with residential and commercial land use  
15 located to the north. The site in Detling was located on the top of a 10 m mast at an  
16 established air quality measurement site in a pasture field approximately 2 km from the  
17 nearest major roads.

### 18 **2.3 GHG measurements**

19 Continuous measurements of CO, CO<sub>2</sub>, CH<sub>4</sub> and water vapour were taken between 1<sup>st</sup> June  
20 and 30<sup>th</sup> September 2012 for the Hackney, Poplar and Teddington sites and 5<sup>th</sup> July to 30<sup>th</sup>  
21 September 2012 at Detling. Each site was instrumented with a G2401 Picarro cavity ring-  
22 down spectroscopy (CRDS) instrument that logged data every 5 seconds and sent data files  
23 each hour to a remote server.

24 All sensors across the network were manually calibrated on an approximately two-weekly  
25 basis using the same gas standards, ensuring the consistency of the measurements from  
26 different sites. The sensors were calibrated for linearity, repeatability of measurements (for  
27 zero and span gases, i.e., respectively with concentrations zero and close to ambient air) and  
28 drift in the field and in the laboratory prior to deployment. The synthetic standards including  
29 the zero and span gases were prepared by National Physical Laboratory (NPL) as described in  
30 Brewer et al. (2014) with mole fractions close to those of atmospheric ambient air ( $379 \pm 0.95$   
31 parts per million (ppm) for CO<sub>2</sub> and  $1800 \pm 5$  parts per billion (ppb) for CH<sub>4</sub>; uncertainties



1 being expressed as 1-sigma standard deviations, STD). A higher than ambient concentration  
2 of CO was used ( $9.71 \pm 0.015$  ppm to be compared to the CO measurements of this study  
3 which range between 0.1 and 0.9 ppb), because of the unavailability of low CO standards at  
4 the time of the experiment, leading to high uncertainties in CO measurements in ambient air.  
5 However, the linearity of the G4201 CRDS has been evaluated by Zellweger et al. (2012)  
6 from 0 up to 20 ppm and their results show that the CRDS analyser remains linear in this  
7 range of concentrations.

8 To quantify possible biases, and consistent with the recommendation from the World  
9 Meteorological Organisation (WMO) Expert group, the design of the experiment should have  
10 included regular measurements of a calibrated target gas. However, the fact that we were  
11 using similar analysers at the four stations, operated with the same protocols and calibrated  
12 with a single reference scale, reduced the risk of systematic biases between the sites. The high  
13 1-sigma uncertainties in the molar fraction of the gases used for the calibration result in biases  
14 that are common to all sites for the measurement period since the same gas cylinders were  
15 used for all stations throughout the period (the calibration error due to uncertainty in the  
16 calibration gas depends on the ambient concentration, but this dependence is such that the  
17 resulting variability of the calibration error is clearly negligible compared with the variability  
18 of the concentrations in time or between sites). For this reason, the calibration biases mostly  
19 cancel out when analysing gradients of ambient molar fractions between the different sites of  
20 the network (this may not hold for higher molar fractions). This bias precludes, however, the  
21 use of this network in combination with other stations that have a different calibration  
22 standard.

23 In addition, the measurement error had a random component of STD 0.3 ppm for CO<sub>2</sub>, 8 ppb  
24 for CH<sub>4</sub> and 15 ppb for CO. This error budget includes drifts and variability in readouts when  
25 measuring zero and span gases, as well as the applied correction for water vapour on the CO<sub>2</sub>  
26 and CH<sub>4</sub> channels. The airstream to the Picarro CRDS was not dried so the measurements of  
27 CO<sub>2</sub> and CH<sub>4</sub> were taken from the dry channel of these analysers to which a default correction  
28 had been applied for variability due to water vapour (Rella et al., 2013). The uncertainty  
29 associated with applying the water vapour correction to this type of instrument, for an H<sub>2</sub>O  
30 content of 1.5%, was estimated to be 0.05 ppm for CO<sub>2</sub> and 1 ppb for CH<sub>4</sub> (Laurent et al.,  
31 2015). No water correction was applied for CO. Expressed as a percentage of the mean  
32 measured concentration throughout the measurement period, the total measurement

1 uncertainties (root mean square, RMS, of the bias and random errors) are 0.3%, 0.7% and  
2 21% for CO<sub>2</sub>, CH<sub>4</sub> and CO, respectively.

3 Data were calibrated using the standard gas cylinder values, and provided as 15-minute  
4 averages by NPL. Calibration episodes were removed from the final dataset. The Teddington  
5 sensor was inactive between 6<sup>th</sup> and 12<sup>th</sup> July due to sample pump failure and there were a  
6 small number of missing days at Detling (due to power outage) and at Poplar (for unknown  
7 reasons). There were few missing data at the Hackney site. The 15-minute data from the  
8 measurement sites were aggregated by averaging into hourly time intervals for comparison  
9 with the hourly output from the model. If fewer than four 15-minute data points were  
10 available for any given hour (usually as a result of periodic data scan by the Picarro analyser  
11 or return to functionality after a calibration event or instrument downtime), the corresponding  
12 hourly average was removed from the analysis to maintain consistency between the model  
13 and data hourly averaged values.

#### 14 **2.4 Simulation of the atmospheric transport of CO<sub>2</sub> and CH<sub>4</sub>**

15 To model the transport of CO<sub>2</sub> and CH<sub>4</sub> mole fractions over London, we used a “South of  
16 England” configuration of the mesoscale atmospheric transport model CHIMERE (Schmidt et  
17 al., 2001). This model has already been used for CO<sub>2</sub> transport and flux inversion at regional-  
18 to-city scale (Aulagnier et al., 2010;Broquet et al., 2011;Bréon et al., 2015). The domain over  
19 which CHIMERE was applied in this study (area ~ 49.9–53.2°N, –6.4–2.4°E) covers the  
20 whole south of England to minimise the impact of defining model boundary conditions using  
21 coarser model simulations close to the measurement sites. Additionally, the boundaries were  
22 traced as much as possible in the seas, in particular the western boundary from which the  
23 dominant winds flow over England. However, the northern boundary crosses England and the  
24 south-eastern part of the domain overlaps a small part of Northern France.

25 The model has a regular grid with 2-km horizontal resolution and 20 vertical levels from the  
26 ground up to 500 hPa (with ~ 20–25 m vertical resolution close to the ground). CHIMERE is  
27 driven by atmospheric mass fluxes from the operational analyses of the European Centre for  
28 Medium-Range Weather Forecasts (ECMWF) at 3 hour and ~ 15-km horizontal resolution  
29 (which are interpolated linearly on the CHIMERE grid and every hour). In this study, these  
30 mass fluxes were processed before their use in CHIMERE to account for the increased  
31 roughness in cities and in particular in London: the surface wind speed was decreased

1 proportionally to the fraction of urban area in each model  $2 \times 2$  km grid cell (i.e., it is set to 0  
2 for grid cells entirely covered by urban area, set to the value from ECMWF for grid cells with  
3 no fraction of urban area, and, in a general way, set to the product of the fraction of non-urban  
4 area in the grid cells times the value from ECMWF). The fraction of urban area within each  $2$   
5  $\times 2$  km grid cell was derived from the land cover map of the Global Land Cover Facility  
6 (GLCF)  $1 \times 1$  km resolution database from the University of Maryland. This database is based  
7 on the methodology of Hansen and Reed (2000) and the Advanced Very High Resolution  
8 Radiometer (AVHRR) data. The decreases in horizontal wind speed are balanced by an  
9 increase of the vertical component of the wind. However, the current configuration does not  
10 account for the urban heat island either in the ECMWF product or in the processing of this  
11 product before its use by CHIMERE.

12 The simulations were initialised on 15<sup>th</sup> April, 2012. For the CO<sub>2</sub> simulations, the initial mole  
13 fractions and the open boundary conditions (at the lateral and top boundaries of the model)  
14 were imposed using simulated CO<sub>2</sub> from the Monitoring the Atmospheric Composition and  
15 Climate Interim Implementation (MACC-II, 2012) forecasts at ~80-km resolution globally  
16 (Agustí-Panareda et al., 2014). The MACC-II forecast was initiated on 1<sup>st</sup> January, 2012 with  
17 online net ecosystem exchange (NEE) from the CTESSEL model (see the description below  
18 of the estimate of natural fluxes used for the CHIMERE simulations) and prescribed fossil  
19 fuel CO<sub>2</sub> emissions and air-sea fluxes, and is not constrained by CO<sub>2</sub> observations. For the  
20 CH<sub>4</sub> with CHIMERE, the initial and boundary conditions were imposed homogeneously in  
21 space and time to be equal to 1.87 ppm, according to the typical mole fractions measured at  
22 the Mace Head atmospheric measurement station in 2012 (NOAA., 2013). The top boundary  
23 conditions were set to a smaller value: 1.67 ppm.

24 Anthropogenic emissions of CO<sub>2</sub> and CH<sub>4</sub> were prescribed to CHIMERE within its domain  
25 using the NAEI emission inventory described in Sect. 2.1. Three-dimensional hourly  
26 emissions for CO<sub>2</sub> and CH<sub>4</sub> were interpolated from this inventory on the 2-km horizontal  
27 resolution model grid. The derivation of the emissions for the UK based on the NAEI  
28 inventory included injection heights for major point sources and temporal profiles (see below  
29 the details on the definition of injection heights and temporal profiles). The CO<sub>2</sub> emissions for  
30 the small part of France appearing in the domain were derived from the Emission Database  
31 for Global Atmospheric Research (EDGAR, 2014) at  $0.1^\circ$  horizontal resolution for the year  
32 2008. Injection heights and temporal variations were ignored for this part of France.

1 The definition of injection heights can have a large impact when modelling the transport of  
2 CO<sub>2</sub> mole fractions from combustion point sources (Bieser et al., 2011). Many parameters  
3 underlying the effective injection heights for each source are not available (e.g., the stack  
4 heights, the flow rate and the temperature in the stacks). Furthermore, this study focuses on  
5 data during summer, and, as indicated later, during the afternoon when the troposphere is  
6 well-mixed, so that the impact of the injection heights is minimum. Therefore, we derived  
7 approximate values for these heights as a function of the sectors associated with the point  
8 sources only, and based on the typical estimates by sector for nitrogen oxide gases (NO<sub>x</sub>), CO  
9 and SO<sub>2</sub> (and for neutral atmospheric temperature conditions) from Pregger and Friedrich  
10 (2009). The resulting injection heights for the emissions listed as point sources by the NAEI  
11 inventory (other emissions were prescribed at ground level) ranged from the second vertical  
12 CHIMERE level (~ 25 to 55 magl) for the smallest industrial and commercial combustion  
13 plants to the 8<sup>th</sup> vertical CHIMERE level (~ 390 to 490 magl) for the power stations. All CH<sub>4</sub>  
14 emissions sources were prescribed at ground level.

15 The variations of CO<sub>2</sub> and CH<sub>4</sub> in time are strongly driven by those of the emissions at the  
16 hourly to the seasonal scale (Reis et al., 2009). In the modelling framework of this study,  
17 temporal profiles were derived for the three sectors of CO<sub>2</sub> emissions with the largest  
18 variations in time: road transport, power generation in large combustion plants, and residential  
19 and commercial combustion. They were based on Reis et al. (2009) using data from 2004 to  
20 2008. These sectorial profiles were applied homogeneously in space for the whole South of  
21 England. For road transport, the profiles were based on the combination of monthly variations  
22 for a typical year, daily variations for a typical week and hourly variations for each day of the  
23 week (with two maxima during week days and one maximum for Saturdays and Sundays)  
24 derived from statistical data about the traffic flows in the UK. For the power generation and  
25 residential and commercial combustion, only monthly variations were considered based on  
26 the consumption for typical years. Previous studies have diagnosed some seasonality for CH<sub>4</sub>  
27 emissions (Lowry et al., 2001;McKain et al., 2015). Indeed, as examples, the seasonality of  
28 the gas consumption for heating (with large consumption for lower temperatures, especially in  
29 winter) could drive seasonal variations in the gas leakage (Jeong et al., 2012), and the  
30 seasonal variations of the meteorology (pressure, humidity, temperature) could impact the  
31 decomposition and release of CH<sub>4</sub>, and thus the emissions, from the waste storage and waste  
32 treatment sector (Börjesson and Svensson, 1997;Masuda et al., 2015;Abushammala et al.,  
33 2016). However, characterizing such seasonal variations is a difficult task, which may vary

1 substantially depending on the sectors and cities. To our knowledge, there are no studies on  
2 which we could build reliable temporal profiles for the CH<sub>4</sub> emissions in London, and we thus  
3 did not attempt to derive it. Instead, we set the CH<sub>4</sub> emissions constant in time.

4 Natural fluxes of CO<sub>2</sub> were taken from the 15 km resolution NEE product from ECMWF  
5 (Boussetta et al., 2013), which is calculated online by the CTESSEL land surface model  
6 coupled with the ECMWF numerical weather prediction model. The CTESSEL model does  
7 not have a specific implementation for urban ecosystems and due to its moderate horizontal  
8 resolution, we cannot expect this model to provide a precise representation of the role of  
9 ecosystems within London.

10 Ocean fluxes for both gases within the domain were ignored because they are assumed to be  
11 negligible at the timescales considered in this study. At the spatial and temporal scales  
12 considered in this study, the loss of CH<sub>4</sub> through chemical reactions is also negligible and was  
13 thus ignored here.

14 The model tracks the transport of the total CO<sub>2</sub>, but also of its different components  
15 separately: CO<sub>2</sub> from the boundaries (BC-CO<sub>2</sub>), from the NEE (BIO-CO<sub>2</sub>) and from fossil-  
16 fuel emissions (FF-CO<sub>2</sub>). The model does not track CO mole fractions; however, the CO  
17 measurements are used to evaluate the FF-CO<sub>2</sub> in Sect. 3.7.

18 The 15-km resolution of the ECMWF analyses, used as meteorological forcing for  
19 CHIMERE, yields relatively uniform wind speed and direction at the city scale. The  
20 interpolation of this product on the 2-km CHIMERE grid is compared with the observations  
21 from surface meteorological sites located in and around London in Sect. 3.3.

## 22 **2.5 Meteorological measurements**

23 An important contribution to model–data discrepancies can arise from errors in the  
24 representation of meteorological conditions; particularly wind speed and direction, and  
25 mixing layer height. To evaluate the meteorological forcing of CHIMERE, hourly  
26 observations of wind speed and direction were collected from the UK Met Office Integrated  
27 Data Archive System (MIDAS) (UK Meteorological Office, 2012). The measured wind data  
28 were obtained for 10 magl at Heathrow Airport, London (51° 28' 43.32", -0° 26' 56.54") and  
29 East Malling, Kent (51° 17' 15.36", 0° 26' 54.24"). East Malling is located 6 km from the  
30 Detling site and Heathrow is located 7 km from the Teddington site and 18 km from the  
31 Hackney and Poplar sites. The locations of the meteorological sites are shown in Fig. 1.

1 Observed winds at East Malling were compared with winds from ECMWF (interpolated on  
2 the CHIMERE grid) at the lowest level (0–25 m) and at the corresponding horizontal location  
3 of the CHIMERE grid. Observed winds at Heathrow were compared with the next CHIMERE  
4 level up (25–50 m) because the urban roughness correction had been applied to the lowest  
5 level. This avoids strong biases in the model–data comparison that would arise because the  
6 urban roughness correction was necessarily applied in a homogenous way for the  
7 corresponding model grid cell, while, in reality the site is not located within the urban canopy.

8 Hourly mean mixing height measurements were collected from a Doppler lidar that was  
9 located on the grounds of a school in North Kensington ( $51^{\circ} 31' 13.97''$ ,  $-0^{\circ} 12' 50.85''$ ) as  
10 part of the Clearflo project (Bohnenstengel et al., 2014). The limited sampling rate of the lidar  
11 was accounted for using a spectral correction method described in Barlow et al. (2014) and  
12 Hogan et al. (2009). Mixing heights were calculated based on a threshold value of the vertical  
13 velocity variance, perturbed between 0.080 and 0.121  $\text{m}^2 \text{s}^{-1}$ . Mean, median, 5<sup>th</sup> and 95<sup>th</sup>  
14 percentile values were calculated for each hour based on these perturbations, and account for  
15 both measurement and method uncertainties (Barlow et al., 2014;Bohnenstengel et al., 2014).  
16 Based on the 5<sup>th</sup> and 95<sup>th</sup> percentile data averaged across all data for each hour, estimated  
17 measurement and method uncertainty was between 53 and 299 m throughout the daily cycle,  
18 with the highest uncertainties usually overnight. These measurement uncertainties are small  
19 when compared with the amplitude of the observed diurnal cycle shown in Fig. 3a. Lidar data  
20 were available for the period between 23<sup>rd</sup> July, 2012 and 17<sup>th</sup> August, 2012 and were  
21 compared with the modelled boundary layer height (diagnosed in the ECMWF forecast using  
22 a critical value of 0.25 for the bulk Richardson number) at North Kensington during this  
23 period.

24

### 25 **3 Results and discussion**

26 The data used for all statistical diagnostics of the model–data discrepancies in this section  
27 (including the wind roses and mean diurnal cycles in Fig. 2 and 3) are for the period 5<sup>th</sup> July  
28 to 30<sup>th</sup> September, 2012 since data were available at all GHG sites during this period. The  
29 analyses of model–data discrepancies in GHG mole fractions utilise the hourly average of the  
30 15-minute aggregate measurements (Sect. 2.3) and the analyses of meteorological  
31 measurements relate to hourly data for the same period. However, some of the figures with  
32 time series of the GHG concentrations display the GHG available data in June 2012.

1 Hereafter, we use the term “signature” to refer to the positive or negative amount of  
2 atmospheric gas mole fraction (and to its spatial and temporal variations) due to a given flux  
3 (natural or anthropogenic surface source or sink over a given area and over a given time  
4 period, or advection of an air mass from a remote area).

### 5 **3.1 First insights on the influence of local sources on urban GHG** 6 **measurements**

7 We first consider the representativity of the CO<sub>2</sub> and CO at the urban sites by analysing them  
8 as a function of wind speed and direction. In particular, we try to give a first assessment of the  
9 weight in the measurements of “local” sources. By local sources, we refer to sources that are  
10 located at distances from the measurement sites that are shorter than the distances over which  
11 we can simulate the transport from these sources at the spatial resolution of our Eulerian  
12 model. This includes sources at less than 1–5 km from the measurement sites since the model  
13 has a 2-km horizontal resolution. Figure 2 shows wind roses at Hackney and Poplar for  
14 measured CO and CO<sub>2</sub>, and modelled CO<sub>2</sub>, alongside aerial images of the site locations. To  
15 reduce the influence of boundary layer variation on the measured and modelled mole  
16 fractions, and to anticipate the data selection on which the study will focus, we include  
17 measured and modelled data for the afternoon period only (see Sect. 3.2).

18 At Hackney there is a clear increase in measured CO and CO<sub>2</sub> mole fractions during periods  
19 of south-easterly wind (Fig. 2a and b). A busy roundabout is located approximately 10 m to  
20 the south-east of the Hackney site with an A-road running from north to south to the east of  
21 the sensor location (Fig 2d). There is no increase for south-easterly winds when analysing  
22 modelled CO<sub>2</sub> (Fig. 2c) suggesting that the observed increase in the measurements could be  
23 related to the roundabout whose specific influence cannot be represented at the 2-km  
24 resolution in the model.

25 At Poplar, the measured CO and CO<sub>2</sub> is more uniform than at Hackney (Figs. 2e and f). It is  
26 still higher in the east but there is no clear signature of the busy roads to the north and south  
27 of the site (Fig. 2h). The modelled CO<sub>2</sub> at Poplar (Fig. 2h) is very similar to that of Hackney  
28 (Fig. 2c), which can be explained by the proximity between the two corresponding model grid  
29 cells (Fig. 1). This supports the earlier assumption that the high mole fractions obtained at  
30 Hackney for south-easterly winds are related to a local source. These analyses also raise a  
31 more general assumption that while the model simulates the signature of emissions at a

1 relatively large scale (due to handling emissions and transport at 2-km resolution and with  
2 significant numerical diffusion) in the area of these 2 sites, there are likely local scale  
3 unresolved emissions strongly influencing observed CO<sub>2</sub> at both urban sites.

4 At both sites the observed CH<sub>4</sub> wind roses are very similar, showing increased mole fractions  
5 towards the east of the sites (data not presented); however, mole fractions are greater in  
6 magnitude at Poplar than at Hackney. Similarly to CO<sub>2</sub>, the model simulates lower CH<sub>4</sub> mole  
7 fractions than observed, with a similar distribution at both sites. The stronger similarity  
8 between the wind roses at the two sites when considering CH<sub>4</sub> measurements than when  
9 considering CO<sub>2</sub> measurements could be explained by the absence of strong CH<sub>4</sub> local  
10 sources in the vicinity of the measurement sites. Indeed, the NAEI inventory does not locate  
11 any major waste treatment facility at less than 5 km from these sites and it assigns a level of  
12 emissions from the other sectors (which are characterised by diffuse sources in the inventory)  
13 for this vicinity that is similar to the general level of CH<sub>4</sub> emissions in the London urban area.  
14 Local CH<sub>4</sub> leaks from the gas distribution could occur and impact the measurements but this  
15 analysis does not highlight such local sources.

16 Despite the potential influence of local sources that are unresolved by the transport model, we  
17 attempt, in the following, to understand and decompose the large discrepancies between the  
18 model and the measurements illustrated in Fig. 2. The objective is to analyse whether one can  
19 identify the discrepancies due to errors in the emissions at scales larger than  $2 \times 2 \text{ km}^2$  which  
20 should give insights on the potential for applying atmospheric inversion.

21

### 22 **3.2 CO<sub>2</sub>, CH<sub>4</sub> and mixing layer mean diurnal cycles**

23 The mean observed and modelled diurnal cycles of the CO, CO<sub>2</sub> and CH<sub>4</sub> mole fractions at  
24 the four GHG measurement sites and the mixing layer height at North Kensington (see Sect.  
25 2.5) are presented in Fig. 3. The amplitude of the mean diurnal cycle in mixing layer height  
26 (Fig. 3a) is approximately 1500 m, typical of summer convective conditions in an urban area  
27 (Barlow et al., 2014).

28 Observed CO<sub>2</sub> mole fractions at all sites follow a typical mean diurnal cycle (Fig. 3) with  
29 maximum mole fractions in the early morning (approx. 05:00, UTC being used hereafter) and  
30 minimum mole fractions during the afternoon (approx. 15:00), which can be related to the  
31 typical variation in mixing height (Fig. 3a), and in vegetation CO<sub>2</sub> exchanges (with



1 photosynthesis and a CO<sub>2</sub> sink during daytime but CO<sub>2</sub> emissions during night-time) during a  
2 daily cycle. The early morning peak in CO<sub>2</sub> mole fractions occurs on average an hour later at  
3 the inner city sites (06:00) compared with the rural and suburban sites (05:00) as shown in  
4 Figs. 3c and 3e. This may be due to the signature of working-week urban emissions with a  
5 peak in traffic around 06:00 to 09:00. This is supported by large observed CO mole fractions  
6 at the urban sites with substantial early morning and evening peaks (Fig. 3b). The peak in CH<sub>4</sub>  
7 measured mole fractions occurs at around 06:00 at all sites (Figs. 3d and 3e).

8 At all sites the model underestimates by 1 to 5% (by 5 to 9 ppm for CO<sub>2</sub> and by 13 to 29 ppb  
9 for CH<sub>4</sub>) the mean observed CO<sub>2</sub> and CH<sub>4</sub> mole fraction during the afternoon hours (12:00 to  
10 17:00), with the highest biases at Hackney for CO<sub>2</sub> and at Poplar for CH<sub>4</sub> (see the model–data  
11 biases for this period in Table 1). This underestimation is consistently larger than the  
12 confidence intervals for the averaging (associated with the limited time sampling) indicated  
13 throughout Fig. 3. The underestimation continues throughout the diurnal cycle at Detling and  
14 Teddington (Figs. 3c and d); however, at the urban sites (Figs. 3e and f), the night-time (00:00  
15 to 05:00) CO<sub>2</sub> and CH<sub>4</sub> mole fractions are considerably larger in the model than in the  
16 observations. This leads to excessively strong diurnal variations at the urban sites, with the  
17 exception of CH<sub>4</sub> at Poplar (Fig. 3f).

18 On average, mixing layer height is underestimated in the model at North Kensington by  
19 approximately 13% (46 m) of the equivalent lidar measurement during the night and 33%  
20 (583 m) during the afternoon (Fig. 3a). There is a high daily variability in the mixing layer  
21 height model–lidar measurement discrepancies (with a 454 m STD in the 12:00–17:00 period  
22 and a 394 m STD in the 00:00 to 05:00 period) and thus this underestimation is not systematic  
23 (see Sect. 3.4). However, this may still explain the overestimation of mole fractions at the  
24 urban sites during night-time but cannot explain the underestimation of CO<sub>2</sub> and CH<sub>4</sub> mole  
25 fractions during the afternoon.

26 Accurate modelling of the boundary layer height in meteorological models is an on-going  
27 concern, particularly in urban areas (Gerbig et al., 2008; Lac et al., 2013) and description of  
28 nocturnal stratification is weak in atmospheric transport models (Geels et al., 2007). During  
29 the night there can be a considerable urban heat island in London as shown for North  
30 Kensington and rural Chilbolton by Bohnenstengel et al. (2014). The model used in our study  
31 does not currently have an urban land-surface scheme capable of reproducing the urban heat  
32 island effects on atmospheric transport (Sect. 2.4). This may explain the different sign of the

1 model–data discrepancies during night-time between the urban sites and the other sites. We  
2 thus restrict the remaining analyses in this paper to the period between 12:00 and 17:00,  
3 wherein we can expect the boundary layer to be well developed, to have a stable height and to  
4 exert minimum influence on the variations in gas mole fractions (Geels et al., 2007; Göckede  
5 et al., 2010).

### 6 **3.3 Comparison between modelled and measured winds**

7 This section focuses on the horizontal wind, which is a critical driver of day to day variations  
8 in GHG mole fractions. We aim to validate the model wind forcing through comparison with  
9 meteorological sites described in Sect. 2.5. The analyses (using hourly data) of measured and  
10 modelled wind are restricted to between 12:00 and 17:00 because all further GHG analyses  
11 are focused on this afternoon period (Sect. 3.2).

12 At East Malling, on average, the model underestimates wind speed by  $0.50 \text{ m s}^{-1}$  (12% of the  
13 observation mean) and wind direction by  $6.90^\circ$  (defining positive angles clockwise hereafter).  
14 The RMS of the hourly model–data discrepancies is  $1.10 \text{ m s}^{-1}$  for wind speed and  $26^\circ$  for  
15 wind direction. At Heathrow Airport, there is an average positive bias of  $0.37 \text{ m s}^{-1}$  (7% of  
16 observation mean) and  $5^\circ$  for wind speed and direction respectively (RMS model–data  
17 discrepancies of  $1.27 \text{ m s}^{-1}$  and  $2.24^\circ$  for wind speed and direction respectively). Some of this  
18 discrepancy may arise from the necessity of comparing the 25–50 m average wind data from  
19 the model to the 10 m height measurements at the Heathrow meteorological station.

20 It is highly difficult to translate such statistics of the errors on the wind into typical errors on  
21 the simulation of the GHG concentrations at the GHG measurement sites since there is a  
22 complex relationship between them, which strongly depends on the specification of the local  
23 to remote emissions, and on the spatial distribution of the errors in the meteorological  
24 parameters or in these emission estimates at the local to larger scales. The overestimation of  
25 the wind speed in the urban area, unlike the underestimation of the mixing layer height, could  
26 partly explain the underestimation of the afternoon GHG concentrations at the urban sites  
27 since it should lead, on average, to an underestimation of the signature of the urban emissions.  
28 However, this overestimation of the wind speed is relatively small.

29 Lac et al. (2013) employed the Meso-NH meteorological model at 2-km horizontal resolution  
30 with an urban surface scheme that models specific energy fluxes between urban areas and the  
31 atmosphere. Their modelled meteorology was compared with hourly meteorological

1 measurements in the Paris region. They showed a typical bias of  $0.8 \text{ m s}^{-1}$  for wind speed and  
2  $20^\circ$  for wind direction, which is worse than the agreement obtained here with the ECMWF  
3 winds driving CHIMERE at a native resolution of 15-km. Nehr Korn et al. (2013) found a  
4 wind speed bias of between  $-1$  and  $2.5 \text{ m s}^{-1}$  and RMS of between 1 and  $4 \text{ m s}^{-1}$  when  
5 comparing the WRF model at 1.33-km resolution over Salt Lake City, US, with an urban land  
6 surface scheme to local hourly wind measurements. Therefore, the choice of a 15-km wind  
7 field to force the CHIMERE transport model over London does not seem to raise typical wind  
8 errors larger than when using a state of the art meteorological model at kilometric resolution.

### 9 **3.4 Daily CO<sub>2</sub> and CH<sub>4</sub> mole fractions during the mid-afternoon**

10 The average CO<sub>2</sub> and CH<sub>4</sub> mole fractions for the afternoon of each day throughout the  
11 analysis period are presented in Figs. 4 and 5. Some data have been excluded from these  
12 analyses; we ignore hereafter, at a given site, any hour during which either modelled or  
13 measured data were not available. We have also excluded data from 29<sup>th</sup> August and 23<sup>rd</sup> to  
14 24<sup>th</sup> September since the model simulated very large GHG peaks on these days which do not  
15 occur in the data. Data from June have been excluded from the statistical analysis to maintain  
16 comparability with Detling at which data were not available during this month.

17 According to both the measurements and the model, there is a clear increase in both the mean  
18 value (typically by 7 ppm and 26 ppb according to the measurements) and variability  
19 (typically by 1 ppm and 16 ppb according to the measurements) of CO<sub>2</sub> and CH<sub>4</sub> mole  
20 fractions, from the rural and suburban Detling and Teddington sites (Figs 4a, 4d, 5a and 5d) to  
21 the urban sites Hackney and Poplar (Figs. 4b, 4c, 5b and 5c). This can be explained by their  
22 relative distance to the main area of anthropogenic emission in the centre of London (Fig. 1)  
23 and due to the location of Teddington (Detling) to the south-west (south-east) of the London  
24 area while the dominant wind directions are from the west. According to the model, in  
25 general, modelled CO<sub>2</sub> is lower than the signature of the MACC-II boundary conditions (BC-  
26 CO<sub>2</sub> in Fig. 4) at Detling and Teddington (by  $\sim 3$  ppm on average) since the negative  
27 signature of the CO<sub>2</sub> NEE is larger than the positive signature of the anthropogenic emissions  
28 between the model boundaries and these sites (see Fig. 4a) and d)). The London emissions  
29 between Detling or Teddington and Hackney or Poplar compensate for this decrease (see Fig.  
30 4b) and c)) in such a way that CO<sub>2</sub> at Hackney and Poplar is generally similar to BC-CO<sub>2</sub>  
31 (with less than 1 ppm difference on average over July–August), except in September when it

1 is higher (by  $\sim 5$  ppm on average) because of the NEE being weaker in this month than during  
2 the previous months. Furthermore, the NEE and the anthropogenic emissions do not strongly  
3 alter the CO<sub>2</sub> variability from the boundary conditions and the correlation between the  
4 variations of modelled hourly CO<sub>2</sub> and those of hourly BC-CO<sub>2</sub> is high (between 0.75 and  
5 0.85, depending on the site) even at urban sites. The modelled CH<sub>4</sub> time series, which uses a  
6 constant value at the boundaries, cannot show such a dependency on the model boundary  
7 conditions (Fig. 5).

8 Statistical comparisons between modelled and measured hourly CO<sub>2</sub> and CH<sub>4</sub> mole fractions  
9 are given in Table 1. While the magnitude of the STD of the model–data discrepancies is  
10 similar to that of the bias for CO<sub>2</sub>, it is far larger than the bias for CH<sub>4</sub>. The RMS of CO<sub>2</sub>  
11 model–data discrepancies is highest at Hackney (12 ppm) but similar at the other three sites (8  
12 to 9 ppm, Table 1). Higher RMS of CH<sub>4</sub> model–data discrepancies are found at Poplar and  
13 Hackney (48 and 55 ppb) than at Teddington and Detling (32 and 33 ppb) (Table 1). The  
14 model–data discrepancies are substantially larger than measurement errors for both CO<sub>2</sub> and  
15 CH<sub>4</sub> (Table 1) so we can exclude measurement error as a key source of the discrepancies. The  
16 discrepancies should thus mainly be associated with representation errors (Sect. 3.1), transport  
17 errors (Sect. 3.3), errors in the domain boundary-conditions and in the prescribed fluxes  
18 within the domain and outside the London area, or with errors in the emissions prescribed in  
19 the London area (based on NAEI data, see Sect. 2.1). The model–data CO<sub>2</sub> or CH<sub>4</sub> hourly  
20 discrepancies at the urban sites during the afternoon are not significantly correlated  
21 (correlations are comprised between 0 and 0.2 for all cases) with the mixing layer height  
22 model–lidar measurement discrepancies at North Kensington (Sect. 3.2) or with the wind  
23 speed or direction model–data discrepancies at Heathrow Airport (Sect 3.3).

24 Model–data correlations are significantly higher for hourly CH<sub>4</sub> (between 0.4 and 0.6,  
25 depending on the sites) than for hourly CO<sub>2</sub> (between 0. and 0.1). However, the amplitude of  
26 the variations of hourly CH<sub>4</sub> is strongly different between the model (whose STD is of 15.5 to  
27 18.5 ppb depending on the sites) and the measurements (whose STD is of 32.8 to 51.5 ppb),  
28 which explains the very large model–data discrepancies given in Table 1. The potential  
29 impact of local CH<sub>4</sub> sources near the urban sites (see Sect. 3.1) cannot explain that these  
30 discrepancies are very high at Teddington and Detling even though they can explain that they  
31 are significantly larger at Hackney and Poplar. This suggests that the actual CH<sub>4</sub> conditions  
32 on the boundaries of the modelling domain may have a strong influence on the variations of

1 measured CH<sub>4</sub>, as for CO<sub>2</sub>, but we miss it through the use of constant CH<sub>4</sub> boundary  
2 conditions in the model.

### 3 **3.5 CO<sub>2</sub> and CH<sub>4</sub> gradients between pairs of sites**

4 An increasing number of studies on the atmospheric monitoring of the city emissions focus on  
5 analysing and assimilating measurement gradients (Bréon et al., 2015;McKain et al.,  
6 2015;Turnbull et al., 2015;Wu et al., 2015;Staufer et al., 2016) rather than measurements at  
7 individual sites since it reduces the influence of the GHG fluxes that are outside the city of  
8 interest (of the model boundary conditions and of the fluxes that are outside the city but  
9 within the model domain when analysing model simulations). This assumes that such an  
10 influence has a large spatial and temporal scale and is therefore similar for different  
11 measurement sites in and around this city (Bréon et al., 2015). Here, the strong influence of  
12 boundary conditions on the modelled CO<sub>2</sub>, and the potential issue raised by using a constant  
13 boundary condition for the CH<sub>4</sub> simulations, leads us to assume that uncertainties in both of  
14 the CO<sub>2</sub> or CH<sub>4</sub> boundary conditions can explain a large part of the substantial discrepancies  
15 between observed and modelled GHGs that are diagnosed at the four measurement sites. We  
16 thus analyse the CO<sub>2</sub> or CH<sub>4</sub> gradient between the urban sites and the rural or suburban sites.  
17 Because of this computation, the rural and suburban sites are called hereafter “reference  
18 sites”. This analysis requires data at both the urban and the reference sites for a given hour  
19 and thus adds a new criterion to the data time selection already described and applied in Sect.  
20 3.4. The gradients are henceforth described as follows; Hackney and Detling (HAC–DET),  
21 Hackney and Teddington (HAC–TED), Poplar and Detling (POP–DET) and Poplar and  
22 Teddington (POP–TED).

23 Figure 6 presents the daily afternoon mean gradients of measured and modelled CO<sub>2</sub> and CH<sub>4</sub>  
24 mole fractions ( $\Delta\text{CO}_2$  and  $\Delta\text{CH}_4$ ) alongside the daily afternoon mean gradient of modelled  
25 FF-CO<sub>2</sub> and BIO-CO<sub>2</sub> components ( $\Delta\text{FF-CO}_2$  and  $\Delta\text{BIO-CO}_2$ ) from the model simulation. It  
26 is clear from Fig. 6 that the modelled  $\Delta\text{CO}_2$  closely tracks modelled  $\Delta\text{FF-CO}_2$  (with a 0.80–  
27 0.95 correlation depending on the selected pair of sites), while  $\Delta\text{BIO-CO}_2$  (the average of  
28 which is smaller than 0.9 ppm in absolute value between all pairs of sites) and the influence of  
29 the boundary conditions on these gradients (the average of which is smaller than 0.1 ppm in  
30 absolute value between all pairs of sites) are relatively small, particularly when Teddington is  
31 used as the reference site (Fig. 6). This strongly supports the assumption that the signature of  
32 boundary conditions and fluxes outside the London area operates on a large spatial and

1 temporal scale and is therefore similar between different sites within the London area, even  
2 though this cannot be directly verified from the measurements. We thus expect that both the  
3 modelled and measured gradients between the urban and the reference sites bear a clear  
4 signature of the anthropogenic emissions from the London area.

5 The largest hourly  $\Delta\text{CO}_2$  are observed on the HAC–DET gradient with a mean ( $\pm$  STD) of  $8.2$   
6  $\pm 5.3$  ppm. The hourly POP–DET gradients have a mean ( $\pm$  STD) of  $5.6 \pm 4.6$  ppm. These are  
7 larger than the gradients observed between an 87 m tower in central London and a rural  
8 location by Rigby et al. (2008).

9 The bias, STD and consequently RMS of the model–data discrepancies between modelled and  
10 measured gradients of both  $\text{CO}_2$  and  $\text{CH}_4$  (Table 2) are much reduced compared with the  
11 same metrics at individual urban sites (Table 1). The RMS of the model–data discrepancies is  
12 roughly halved for  $\Delta\text{CO}_2$  compared with site  $\text{CO}_2$  (from 9.0 or 11.7 ppm for the urban sites to  
13 3.6–6.3 ppm for the gradients depending on the corresponding pairs of sites). There is also a  
14 small improvement in correlation between observed and modelled  $\Delta\text{CO}_2$  compared with  
15 correlation between observed and modelled  $\text{CO}_2$  at individual urban sites (from between 0.02  
16 and 0.13 to between 0.20 and 0.35), but model–data correlations for  $\Delta\text{CH}_4$  are reduced  
17 compared with those for  $\text{CH}_4$  at the individual urban sites (from between 0.42 and 0.58 to  
18 between 0.20 and 0.30).

19 The measurements at each site are affected by a constant calibration bias (see Sect. 2.3),  
20 therefore the decrease in model–data biases after the gradient computation partially comes  
21 from the cancellation of this systematic error. However, this systematic error (typically 1 ppm  
22 and 5 ppb for  $\text{CO}_2$  and  $\text{CH}_4$  respectively; Table 1) is much smaller than the difference  
23 between the model–data biases when considering the analysis of mole fractions at individual  
24 sites (Table 1) and those when considering gradients between these sites (Table 2).  
25 Furthermore, the random measurement error should be larger for gradients than at individual  
26 sites (since the gradient computation combines the random measurement errors at individual  
27 sites). Therefore, the main driver of the strong decrease of model–data discrepancies when  
28 analysing gradients instead of mole fractions at individual sites should be the strong reduction  
29 of the large scale errors from the boundary conditions and remote fluxes.

30 The random component of the measurement errors should be uncorrelated between different  
31 sites, and thus the STD of the gradient measurement error should be  $\sqrt{2}$  times the STD of the  
32 measurement error at individual sites. Therefore, the gradient measurement error should

1 remain much smaller (typically equal to 0.4 ppm and 11 ppb for CO<sub>2</sub> and CH<sub>4</sub> respectively)  
2 than the gradient model–data discrepancies (Table 2). The gradient model–data discrepancies  
3 should thus mainly be related to model (transport and representation) errors and errors in the  
4 estimate of fluxes in the London area, unless a significant influence of the remote fluxes  
5 remains in the measured gradients despite the cancelling of such an influence in the model  
6 due to the gradient computation.

### 7 **3.6 CO<sub>2</sub> and CH<sub>4</sub> gradients with wind direction filtering**

8 Figure 6 shows that the fit between the modelled  $\Delta\text{CO}_2$  and  $\Delta\text{FF-CO}_2$  is better for gradients to  
9 Teddington than to Detling. Potential explanations could be that Teddington is far closer to  
10 London’s centre than Detling (Fig. 1), and that Teddington is more frequently upwind of the  
11 city than Detling. The signature of fluxes outside the London area can be assumed to be more  
12 homogeneous along the wind direction than over the whole London area (Bréon et al.,  
13 2015;Staufer et al., 2016), in particular for the measurements (for the model, the boundary  
14 conditions and fluxes outside London are prescribed with relatively coarse resolution  
15 products, see Sect. 2.4, so this signature is homogeneous over larger spatial scales in the  
16 model than in the measurements). Bréon et al. (2015) decreased the signature of the fluxes  
17 outside the city by considering gradients between two sites along the wind direction rather  
18 than by considering the gradients between any two sites in the city area for any wind  
19 condition. We therefore expect the gradients to Teddington to be representative of the London  
20 urban emissions more often than the gradients to Detling. Measured gradients calculated  
21 without considering the wind direction, particularly gradients to Detling, could retain a  
22 significant influence of the boundary conditions and fluxes outside the London area (even  
23 though this does not occur in the model), and this would explain why these measured  
24 gradients sometimes reach negative values (e.g.,  $-10.2$  to  $-20.9$  ppm for CO<sub>2</sub> on July 25 and  
25 Sept 9) even though they were computed to isolate the signature of the London emissions  
26 (Fig. 6).

27 Therefore, to reduce the influence of remote fluxes and increase the signature of the London  
28 urban emission when analysing both the measured and simulated gradients, we next select  
29 gradients for hours in which the corresponding reference site is upwind of the corresponding  
30 urban site. In practice, we select the hourly gradient between an urban site and the reference  
31 site when the wind direction measured at Heathrow (if the reference site is Teddington) or  
32 East Malling (if the reference site is Detling) is within a  $\pm 20^\circ$  range around the direction from

1 the reference site to the urban site (which corresponds to the pink shading on Fig. 6). The  
2 selected gradients correspond to 22% (101 over 452) of the available HAC–TED afternoon  
3 gradients and 22% (93 over 431) of the POP–TED available afternoon gradients for either  
4 CO<sub>2</sub> or CH<sub>4</sub>. There are only 17 hourly (CO<sub>2</sub> or CH<sub>4</sub>) gradients to Detling (3% of all available  
5 afternoon gradients to Detling) recorded wherein Detling was positioned upwind of the urban  
6 sites. Because of this low number of selected observations, gradients to Detling are ignored in  
7 the remainder of the analyses.

8 The statistics of the model–data discrepancies for gradients to Teddington when this site is  
9 upwind the urban sites are presented in Table 2. Filtering for wind direction reduced the  
10 negative bias and the RMS of discrepancies for  $\Delta\text{CO}_2$  HAC–TED gradients, but slightly  
11 increased the RMS of discrepancies and increased the positive bias on the  $\Delta\text{CO}_2$  POP–TED  
12 gradient relative to analysis without wind filtering. The resulting STD of the discrepancies has  
13 values (approx. 2.5–3.5 ppm) that correspond to the typical observation and model transport  
14 errors identified by other inverse modelling studies, e.g., Bréon et al. (2015) diagnose a 3 ppm  
15 STD of the observation error for gradients in the Paris area. However, the bias in  $\Delta\text{CO}_2$  for  
16 both HAC–TED and POP–TED after wind filtering is within the range of 1 to 2 ppm which  
17 remains relatively high. There is an underestimation at Hackney and an overestimation at  
18 Poplar. Regarding  $\Delta\text{CH}_4$ , all the statistics of the model–data discrepancies after wind filtering  
19 are improved substantially, resulting in the RMS discrepancies being roughly halved (from ~  
20 37 ppb to ~ 15 ppb) when comparing the statistics with and without wind filtering.

21 To increase the number of selected gradients and thus the robustness of the statistics, we next  
22 conduct a test wherein the constraint on the wind direction is relaxed to  $\pm 40^\circ$  around the  
23 direction from the suburban to the urban site. The resulting bias and RMS of model–data  
24 discrepancies for  $\Delta\text{CO}_2$  are very similar for HAC–TED to those with a range of  $\pm 20^\circ$  around  
25 the direction from the suburban to the urban site (with bias of  $-1.8$  ppm and RMS of the  
26 discrepancies of 3.4 ppm). However, the  $\pm 40^\circ$  wind direction improves the statistics at Poplar  
27 (with bias of 0.9 ppm and RMS of model–data discrepancies of 3.1 ppm). While this option  
28 yields better results in general, it diverges from the principle of monitoring the gradients of  
29 concentration along the transport direction only.

30 Since local sources have been identified as a potential major source of model–data  
31 discrepancies, a further analysis of the gradients when the wind direction is within a  $\pm 20^\circ$   
32 range around the direction from the suburban to the urban site is conducted by selecting only



1 gradients to Teddington when both the hourly mean wind speed measured at Heathrow and  
2 modelled at Teddington are above  $3 \text{ ms}^{-1}$ . Such a threshold is assumed to decrease the  
3 influence of local sources on the variations of the GHG mole fractions (Bréon et al., 2015).  
4 However, the sensitivity to this selection is relatively weak and it only slightly improves the  
5 results for  $\Delta\text{CO}_2$  and  $\Delta\text{CH}_4$  for HAC–TED (i.e., decreases the RMS discrepancies by 0.3 ppm  
6 for  $\Delta\text{CO}_2$  and 2.1 ppb for  $\Delta\text{CH}_4$ ) and  $\Delta\text{CH}_4$  for POP–TED (i.e., decreases the RMS  
7 discrepancies by 0.4 ppb) and slightly increases the discrepancies for  $\Delta\text{CO}_2$  for POP–TED  
8 (i.e., increases their RMS by 0.2 ppm), while further decreasing the number of observations  
9 (to 82 POP–TED gradients and 87 HAC–TED gradients for either  $\text{CO}_2$  or  $\text{CH}_4$ ) and thus  
10 reducing the robustness of the statistics.

### 11 **3.7 Estimation of the fossil fuel component of the $\text{CO}_2$ mole fractions**

12 While the signature of the fossil fuel emissions dominates and the contribution of the natural  
13 fluxes is weak in the modelled gradient between urban and suburban  $\text{CO}_2$ , especially when  
14 considering POP–TED and HAC–TED gradients filtered according to the wind direction  
15 (Sect. 3.6 and Fig. 6b) and d)), the contribution of the natural fluxes can be significant even  
16 when applying the wind direction filtering for HAC–DET or POP–DET  $\text{CO}_2$  gradients (Fig.  
17 6a) and c)). Furthermore, the C-TESSSEL model used to simulate the  $\text{CO}_2$  NEE does not  
18 correctly represent the NEE in the London area (see Sect 2.4) while the natural fluxes within  
19 urban areas can be significant compared with the anthropogenic emissions (Nordbo et al.,  
20 2012). These points, the discussions in Sect. 3.6, and the residual discrepancies when  
21 comparing measured and modelled gradients question the validity of the assumption that the  
22 signature of the natural fluxes is not significant compared with that of the fossil fuel  
23 emissions in the measured gradient with or without wind direction filtering.

24 In this section we thus attempt to improve the focus on the signature of the urban emissions  
25 by deriving a  $\text{CO}_2$  fossil fuel component from both the modelled and the measured gradients.  
26 While the model directly provides the  $\Delta\text{FF-CO}_2$  values, we use an empirical method based on  
27 the continuous CO measurements to extract an observation based estimate of  $\Delta\text{FF-CO}_2$   
28 between the measurement sites, since CO and  $\text{CO}_2$  are co-emitted when fossil fuels are burnt.  
29 We focus the analysis on HAC–TED and POP–TED when Teddington is located upwind of  
30 the urban sites (with a  $\pm 20^\circ$  margin for the selection of the corresponding wind direction),  
31 given that such a choice increases the consistency between the model and the data (Sect. 3.6).

1 The ratio of CO to FF-CO<sub>2</sub> (henceforth R) varies depending on the different type of sources  
 2 (e.g., traffic, industry) whose relative influence at the measurement sites can vary in time due  
 3 to changing circulation conditions. However, we assume that these relative influences on  
 4 HAC–TED and POP–TED gradients are constant in time during the afternoon when  
 5 Teddington is upwind of the urban sites. We also assume that CO acts as a conservative tracer  
 6 and does not interact with the surrounding environment during its transport throughout the  
 7 London urban area (Gamnitzer et al., 2006). Consequently, we assume that R resulting from  
 8 the combination of all sources is constant for gradients between two given sites. Using CO  
 9 gradients and this ratio, one can derive the observation based ΔFF-CO<sub>2</sub> using the following  
 10 equation (Eq. 1):

$$11 \quad \Delta FF - CO_2 = \frac{CO_{urb} - CO_{suburb}}{R}, \quad (1)$$

12 where CO<sub>urb</sub> is the observed CO mole fractions at the urban site and CO<sub>suburb</sub> is the observed  
 13 CO mole fractions at the suburban Teddington site.

14 We can assume a traffic-dominated value of R during summer as we can anticipate lower  
 15 energy consumption due to natural gas burning in the surrounding area (Vogel et al., 2010).  
 16 Examination of the diurnal cycle of CO at the urban sites revealed the typical traffic-based  
 17 variability of increased mole fractions in the early morning and late afternoon and larger CO  
 18 mole fractions during the day than overnight (Sect. 3.2, Fig. 3b). A value of 0.011 is given to  
 19 R based on the literature that has evaluated traffic dominated values of R in urban areas (in  
 20 Western areas of the world) using the <sup>14</sup>C isotope (Wunch et al., 2009; Vogel et al.,  
 21 2010; Newman et al., 2013). We further assume that the errors in observation based ΔFF-CO<sub>2</sub>  
 22 are smaller than the model or actual ΔFF-CO<sub>2</sub> variations.

23 Modelled ΔFF-CO<sub>2</sub> is on average slightly larger than observation-based ΔFF-CO<sub>2</sub> on the  
 24 HAC–TED gradient (observed-based mean ΔFF-CO<sub>2</sub> ± STD of 6.2 ± 2.3 ppm and modelled  
 25 mean ΔFF-CO<sub>2</sub> ± STD of 5.8 ± 3.8 ppm). On the POP–TED gradient, observation-based ΔFF-  
 26 CO<sub>2</sub> is considerably lower than the modelled ΔFF-CO<sub>2</sub> (observation-based mean ΔFF-CO<sub>2</sub> ±  
 27 STD of 3.5 ± 1.0 ppm and modelled mean ΔFF-CO<sub>2</sub> ± STD of 6.3 ± 2.9 ppm). Statistical  
 28 comparisons between modelled and observation-based ΔFF-CO<sub>2</sub> mole fractions are given in  
 29 Table 3. Compared with ΔCO<sub>2</sub> (Table 2), we see a very strong reduction in bias and RMS on  
 30 the HAC–TED gradient when considering the fossil fuel component only. However, the POP–  
 31 TED gradients model–data bias is significantly increased when comparing results for ΔFF-  
 32 CO<sub>2</sub> to those for ΔCO<sub>2</sub> (Tables 2 and 3).

1

## 2 **4 Concluding remarks**

3

4 In this study we compared observed CO<sub>2</sub> and CH<sub>4</sub> mole fractions from four near ground  
5 measurement sites in and around London to the simulations from a mesoscale transport model  
6 driven by temporally and spatially varying emissions estimates. We aimed to determine  
7 whether these near ground sites would be amenable to the atmospheric inversion of the  
8 London city scale emissions using such an atmospheric transport model. The measurements  
9 and model simulation applied to the period June–September 2012. Given the initial diagnostic  
10 of very large model–data discrepancies at the different measurement sites, this study  
11 attempted to remove or characterise the influence of some of the underlying sources of  
12 uncertainty and to isolate, in both the model and the measurements, the signal that  
13 corresponds to the London anthropogenic emissions, which would be targeted by the  
14 inversion.

15 Focusing the analysis on afternoon data limited the impact of the model’s inability to  
16 correctly predict the transitions of the mixing layer depth in morning and evening. This  
17 problem was acknowledged in other GHG transport studies (Denning et al., 1999; Geels et al.,  
18 2007; Lac et al., 2013). It is possible that this is exacerbated here because of the London urban  
19 heat island, which is significant overnight (Barlow et al., 2014; Bohnenstengel et al., 2014),  
20 while the model meteorological forcing did not include a true urban parameterization.

21 Focusing the analysis on gradients between the urban sites and the reference sites, especially  
22 when selecting them for periods when the suburban reference site was upwind of the urban  
23 sites, strongly reduced the impact of errors from the boundary conditions and fluxes outside  
24 of the London area in the modelling configuration. Since these boundary conditions and  
25 remote fluxes were shown to strongly drive the time variations of the mole fractions in the  
26 London area, this focus yielded a relatively low time-varying component of the model–data  
27 discrepancies. According to the model, this gradient computation also allowed isolating the  
28 signature of the London anthropogenic emissions from that of the natural fluxes in the area.  
29 The very good fit between the modelled fossil fuel CO<sub>2</sub> gradient between Hackney and  
30 Teddington (when Teddington is upwind of Hackney) and the CO measurement based  
31 estimate of this gradient (even though this estimate relied on crude assumptions regarding the  
32 correlation between CO and fossil fuel CO<sub>2</sub>) could further support the assumption that the

1 urban to suburban along-wind gradient bears a very strong signature of the London emissions  
2 that is consistent between the model and the measurements.

3 However, there are large biases between the modelled fossil fuel CO<sub>2</sub> gradient between Poplar  
4 and Teddington (when Teddington is upwind of Poplar) and the CO measurement-based  
5 estimate of this gradient, and between the modelled and measured CO<sub>2</sub> gradients between the  
6 urban and reference sites (filtering or not by the wind direction so that the reference site is  
7 upwind of the urban site). These biases could be related to biases in the estimate of  
8 anthropogenic emissions in the model. However, there is a clear difference between the  
9 measured gradients from Hackney to Teddington and those from Poplar to Teddington, while  
10 the model predicts similar gradients when considering either urban site, either when  
11 considering the average, or the daily variations of the afternoon gradients (Fig. 6b and d). In  
12 particular, this results in model–data biases with opposed signs depending on the urban site  
13 considered. This indicates that such biases and much of the variations in the gradient model–  
14 data discrepancies are likely related to local sources that cannot be represented with the 2-km  
15 resolution model rather than to errors in the city scale estimate of the anthropogenic emissions  
16 in the model. The influence of the local traffic source, identified southeast of the Hackney site  
17 in Sect. 3.1, should be removed from the analysis of gradients to Teddington when  
18 Teddington located upwind i.e., west of Hackney. However, other smaller sources are likely  
19 to occur nearby to the urban sites.

20 For CH<sub>4</sub> there is greater similarity between observations or between the model simulations at  
21 the two urban sites. This suggests that there are no CH<sub>4</sub> local sources near these sites. This  
22 seems reasonable because the major CH<sub>4</sub> point sources in urban environments are mainly  
23 related to a limited number of specific waste processing sites, none of which is located near  
24 the measurement sites by the NAEI inventory, or to points of leakage in the gas distribution  
25 network, which only represent 20% of the CH<sub>4</sub> emissions in the London area according to  
26 Lowry (2001). This, and the poorer representation of the boundary conditions for CH<sub>4</sub> in the  
27 model, can explain why the CH<sub>4</sub> discrepancies were reduced more successfully than the CO<sub>2</sub>  
28 discrepancies when switching from the analysis of data at individual sites to the analysis of  
29 gradients.

30 The errors in the meteorological forcing could also participate to the model–data CO<sub>2</sub> or CH<sub>4</sub>  
31 discrepancies even though the analysis did not identify a direct link between them and the  
32 model–data wind or BLH discrepancies. The biases between this forcing and measured wind

1 in terms of biases in wind speed ( $0.37 \text{ m s}^{-1}$  i.e., 7% of observation mean) and in terms of  
2 biases in wind direction ( $5^\circ$ ) were smaller than reported by other studies (Lac et al., 2013), but  
3 could be highly problematic in a urban environment with highly heterogeneous sources in the  
4 vicinity of the measurement sites (Bréon et al., 2015). The meteorological forcing was also  
5 shown to underestimate the mixing layer depth during the afternoon.

6 Furthermore, we assessed measurement error as a potential source of model–data  
7 discrepancies throughout the analyses. Practical constraints for this short measurement  
8 campaign did not allow us to design it in such a way that the measurements can be compared  
9 with each other or with other measurements within 0.1 ppm, as recommended by WMO for  
10 the northern hemisphere (WMO, 2012). The random measurement error at individual sites  
11 was smaller than the model–data discrepancies by an order of magnitude so was considered to  
12 be negligible. However, the systematic measurement error is large enough not to be neglected  
13 in the raw discrepancies, even though it does not dominate. By definition, the unknown offset  
14 in our network vanishes when inter-site gradients are considered, but only because a unique  
15 calibration cylinder was used for all sites and for the whole measurement period, which is not  
16 a robust solution for larger and longer-lasting local networks. This unknown offset hampers  
17 any comparison with other measurement sites in the UK or other places in the world that can  
18 therefore not be assimilated in the same inverse modelling system as our London city  
19 measurements.

20 As a result, the amplitude of the model–data discrepancies in the gradients is often as large as  
21 that of the measured gradients, in particular for  $\text{CH}_4$ , which is not optimistic regarding the  
22 ability to adjust the estimate of the London urban emissions. McKain et al. (2015) were able  
23 to conduct a city-scale assessment of the emissions of Boston, but this relied on the fact that  
24 the fugitive  $\text{CH}_4$  emissions from the gas distribution network are high in large cities in the US  
25 (Philipps et al. 2013). As indicated above, Lowry et al. (2001) showed that such emissions are  
26 far lower for a city like London and similar conclusions were raised by recent  $\text{CH}_4$  monitoring  
27 campaigns in Paris and Rotterdam within the KIC Climate Carbocount-city project  
28 (<http://www.climate-kic.org/projects/carbon-emissions-from-cities/>). In many cities, including  
29 London, the major  $\text{CH}_4$  emissions do not seem diffuse or significant enough in the urban  
30 environment to be monitored using a city-scale atmospheric inversion approach. Monitoring  
31 individually (using local-scale inversion techniques, (Yver Kwok et al., 2015)) the specific  
32  $\text{CH}_4$  point sources dominating the city emissions and which are often located outside the

1 central urban area (landfills, waste water treatment plants and gas compression sites) may thus  
2 prove to be more suitable than the city-scale approach in these cities.

3 For CO<sub>2</sub>, the fact that the model–data discrepancies in the gradients, which mainly consist of  
4 biases, do not occur at large scale and are likely strongly driven by local sources that cannot  
5 be represented with the 2-km resolution transport model raises strong challenges for the  
6 inversion of the CO<sub>2</sub> emissions using such a transport model. The location of the  
7 measurement sites in the core of the urban area (where the building and traffic is very dense  
8 and the topography is made complex by the urban canopy) close to the ground (at less than 15  
9 magl), where the sensitivity to local sources is very high, may be responsible for such an  
10 issue. Therefore, this study strongly questions the current ability to exploit a GHG network  
11 with near ground urban measurement sites alongside a state of the art atmospheric inversion  
12 system with atmospheric transport models at kilometric horizontal resolution and ignoring the  
13 sub-grid scale variability of such a model.

14 Bréon et al. (2015) and Staufer et al (2016) showed that near ground CO<sub>2</sub> measurements at  
15 less than 20 magl, and located in suburban areas at opposite edges of the urban area, can be  
16 used for city-scale CO<sub>2</sub> inversions assimilating cross-city upwind–downwind gradients.  
17 Exploiting CO<sub>2</sub> measurements at more than 20 magl in the core of the urban area could  
18 remain a challenge due to local transport processes and sources, as shown by the analysis of  
19 Bréon et al. 2015 for the measurements at the top of the Eiffel Tower in Paris. This challenge  
20 may be addressed using networks with different types of urban measurements (e.g. integrated  
21 column measurements, Hase et al. (2015)), or averaging data from sufficiently dense  
22 sampling to obtain information about the spatial scales relevant to the model. Several  
23 conceptual improvements of the inversion methodology could also support the exploitation of  
24 urban measurements and to determine where, under which conditions and/or how the large-  
25 scale signal can be filtered from the measurements so that it could be well represented by the  
26 kilometric-resolution models. This would require the analysis of the representativity of  
27 potential location of the urban measurement sites and of the CO<sub>2</sub> atmospheric variability at  
28 very high resolution using e.g. local high resolution model simulations, mobile measurements,  
29 or a very dense array of measurements in a small area. All these measurements and modelling  
30 concepts remain to be deployed and tested but this still leaves some potential for the  
31 exploitation of near ground urban measurements within city-scale inversion frameworks.

1 Even though this study mainly highlighted the challenges of using near ground urban  
2 measurements, it still strengthened the confidence in specific inversion techniques. The  
3 assimilation of measurement gradients along the wind direction instead of individual  
4 measurements is increasingly used for city-scale activities. However, it is barely used for  
5 larger scale inversion activities. Alternative approaches are used to limit the impact of the  
6 uncertainties in the model boundary conditions, such as the control of the baseline  
7 concentrations for the different measurements sites by the inversion (Lauvaux et al.,  
8 2012;Henne et al., 2016). The improvement brought by the gradient analysis and the issues  
9 encountered with urban measurement strongly supports the potential of this “gradient  
10 approach” and encourages the design of city networks where most stations are located at the  
11 edge of the urban area rather than spread evenly in the core of this area. Finally, the  
12 improvement of the model–data statistics obtained with a simple approach for deriving  
13 observation-based fossil fuel CO<sub>2</sub> gradients from CO gradients demonstrates the need for  
14 accurate partitioning of the natural and anthropogenic atmospheric signals even in a city like  
15 London. This increases confidence in the idea that the joint assimilation of CO and CO<sub>2</sub> data  
16 could strengthen the potential of the inversion for monitoring the anthropogenic emissions,  
17 even though some recent studies highlight the challenge for bringing some constraint to  
18 estimate the (variable) CO/CO<sub>2</sub> anthropogenic emission ratio (Ammoura et al., 2014).

19

## 20 **Acknowledgements**

21 This work was funded and supported by Astrium Services SAS. The authors would like to  
22 thank Brian Sweeney of the National Physical Laboratory for his efforts in keeping the  
23 measurement sites calibrated and well maintained. We would like to thank the Clearflo  
24 project members for provision of the lidar data from their summer IOP at North Kensington  
25 and thanks go to Christos Halios for help with interpreting the lidar data. Thanks also go to  
26 Davey Atkinson for help with figure preparation.

27

## 1 References

- 2 Abushammala, M. F. M., Basri, N. E. A., and Younes, M. K.: Seasonal Variation of Landfill  
3 Methane and Carbon Dioxide Emissions in a Tropical Climate, *International Journal of*  
4 *Environmental Science and Development*, 7, 586-590, 2016.
- 5 Agustí-Panareda, A., Massart, S., Chevallier, F., Boussetta, S., Balsamo, G., Beljaars, A.,  
6 Ciais, P., Deutscher, N. M., Engelen, R., Jones, L., Kivi, R., Paris, J. D., Peuch, V. H.,  
7 Sherlock, V., Vermeulen, A. T., Wennberg, P. O., and Wunch, D.: Forecasting global  
8 atmospheric CO<sub>2</sub>, *Atmos. Chem. Phys.*, 14, 11959-11983, 10.5194/acp-14-11959-2014, 2014.
- 9 Ammoura, L., Xueref-Remy, I., Gros, V., Baudic, A., Bonsang, B., Petit, J. E., Perrussel, O.,  
10 Bonnaire, N., Sciare, J., and Chevallier, F.: Atmospheric measurements of ratios between  
11 CO<sub>2</sub> and co-emitted species from traffic: a tunnel study in the Paris megacity,  
12 *Atmos. Chem. Phys.*, 14, 12871-12882, 10.5194/acp-14-12871-2014, 2014.
- 13 Aulagnier, C., Rayner, P., Ciais, P., Vautard, R., Rivier, L., and Ramonet, M.: Is the recent  
14 build-up of atmospheric CO<sub>2</sub> over Europe reproduced by models. Part 2: an overview with  
15 the atmospheric mesoscale transport model CHIMERE, *Tellus B*, 62, 14-25, 10.1111/j.1600-  
16 0889.2009.00443.x, 2010.
- 17 Barlow, J. F., Halios, C. H., Lane, S. E., and Wood, C. R.: Observations of urban boundary  
18 layer structure during a strong urban heat island event, *Environ Fluid Mech*, 1-26,  
19 10.1007/s10652-014-9335-6, 2014.
- 20 Bieser, J., Auling, A., Matthias, V., Quante, M., and van der Gon, H.: Vertical emission  
21 profiles for Europe based on plume rise calculations, *Environ. Pollut.*, 159, 2935-2946,  
22 10.1016/j.envpol.2011.04.030, 2011.
- 23 Bohnenstengel, S. I., Belcher, S. E., Aiken, A., Allan, J. D., Allen, G., Bacak, A., Bannan, T.  
24 J., Barlow, J. F., Beddows, D. C. S., Bloss, W. J., Booth, A. M., Chemel, C., Coceal, O., Di  
25 Marco, C. F., Dubey, M. K., Faloon, K. H., Fleming, Z. L., Furger, M., Gietl, J. K., Graves,  
26 R. R., Green, D. C., Grimmond, C. S. B., Halios, C. H., Hamilton, J. F., Harrison, R. M.,  
27 Heal, M. R., Heard, D. E., Helfter, C., Herndon, S. C., Holmes, R. E., Hopkins, J. R., Jones,  
28 A. M., Kelly, F. J., Kotthaus, S., Langford, B., Lee, J. D., Leigh, R. J., Lewis, A. C., Lidster,  
29 R. T., Lopez-Hilfiker, F. D., McQuaid, J. B., Mohr, C., Monks, P. S., Nemitz, E., Ng, N. L.,  
30 Percival, C. J., Prévôt, A. S. H., Ricketts, H. M. A., Sokhi, R., Stone, D., Thornton, J. A.,  
31 Tremper, A. H., Valach, A. C., Visser, S., Whalley, L. K., Williams, L. R., Xu, L., Young, D.  
32 E., and Zotter, P.: Meteorology, air quality, and health in London: The ClearfLo project,  
33 *Bulletin of the American Meteorological Society*, 10.1175/BAMS-D-12-00245.1, 2014.
- 34 Börjesson, G., and Svensson, B. H.: Seasonal and Diurnal Methane Emissions From a  
35 Landfill and Their Regulation By Methane Oxidation, *Waste Management & Research*, 15,  
36 33-54, 10.1177/0734242x9701500104, 1997.
- 37 Boussetta, S., Balsamo, G., Beljaars, A., Panareda, A.-A., Calvet, J.-C., Jacobs, C., van den  
38 Hurk, B., Viterbo, P., Lafont, S., Dutra, E., Jarlan, L., Balzarolo, M., Papale, D., and van der  
39 Werf, G.: Natural land carbon dioxide exchanges in the ECMWF integrated forecasting  
40 system: Implementation and offline validation, *Journal of Geophysical Research:*  
41 *Atmospheres*, 118, 5923-5946, 10.1002/jgrd.50488, 2013.
- 42 Bréon, F. M., Broquet, G., Puygrenier, V., Chevallier, F., Xueref-Remy, I., Ramonet, M.,  
43 Dieudonné, E., Lopez, M., Schmidt, M., Perrussel, O., and Ciais, P.: An attempt at estimating



1 Paris area CO<sub>2</sub> emissions from atmospheric concentration measurements, *Atmos. Chem.*  
2 *Phys.*, 15, 1707-1724, 10.5194/acp-15-1707-2015, 2015.

3 Brewer, P. J., Brown, R. J. C., Miller, M. N., Miñarro, M. D., Murugan, A., Milton, M. J. T.,  
4 and Rhoderick, G. C.: Preparation and Validation of Fully Synthetic Standard Gas Mixtures  
5 with Atmospheric Isotopic Composition for Global CO<sub>2</sub> and CH<sub>4</sub> Monitoring, *Analytical*  
6 *Chemistry*, 86, 1887-1893, 10.1021/ac403982m, 2014.

7 Broquet, G., Chevallier, F., Rayner, P., Aulagnier, C., Pison, I., Ramonet, M., Schmidt, M.,  
8 Vermeulen, A. T., and Ciais, P.: A European summertime CO<sub>2</sub> biogenic flux inversion at  
9 mesoscale from continuous in situ mixing ratio measurements, *J Geophys Res-Atmos*, 116,  
10 10.1029/2011jd016202, 2011.

11 Bush, T., Tsagatakis, I., Passant, N., Griffin, A., and Pearson, B.: UK Emission Mapping  
12 Methodology 2007, Didcot, Oxfordshire. ED48954, 52 pp., 2010.

13 Ciais, P., Paris, J. D., Marland, G., Peylin, P., Piao, S. L., Levin, I., Pregger, T., Scholz, Y.,  
14 Friedrich, R., Rivier, L., Houwelling, S., Schulze, E. D., and Team, C. S.: The European  
15 carbon balance. Part 1: fossil fuel emissions, *Glob. Change Biol.*, 16, 1395-1408,  
16 10.1111/j.1365-2486.2009.02098.x, 2010a.

17 Ciais, P., Rayner, P., Chevallier, F., Bousquet, P., Logan, M., Peylin, P., and Ramonet, M.:  
18 Atmospheric inversions for estimating CO<sub>2</sub> fluxes: methods and perspectives, *Clim. Change*,  
19 103, 69-92, 10.1007/s10584-010-9909-3, 2010b.

20 Denning, A. S., Holzer, M., Gurney, K. R., Heimann, M., Law, R. M., Rayner, P. J., Fung, I.  
21 Y., Fan, S.-M., Taguchi, S., Friedlingstein, P., Balkanski, Y., Taylor, J., Maiss, M., and Levin,  
22 I.: Three-dimensional transport and concentration of SF<sub>6</sub>, *Tellus B*, 51, 266-297,  
23 10.1034/j.1600-0889.1999.00012.x, 1999.

24 Dragosits, U., and Sutton, M. A.: Modelling and mapping UK emissions of ammonia,  
25 methane and nitrous oxide from agriculture, nature, waste disposal and other miscellaneous  
26 sources for 2009., 20, 2011.

27 Emissions Database for Global Atmospheric Research:  
28 <http://edgar.jrc.ec.europa.eu/index.php>, access: 13/01/2014, 2014.

29 Font, A., Grimmond, C. S. B., Kotthaus, S., Morgui, J. A., Stockdale, C., O'Connor, E.,  
30 Priestman, M., and Barratt, B.: Daytime CO<sub>2</sub> urban surface fluxes from airborne  
31 measurements, eddy-covariance observations and emissions inventory in Greater London,  
32 *Environ. Pollut.*, 196, 98-106, 10.1016/j.envpol.2014.10.001, 2015.

33 Gamnitzer, U., Karstens, U., Kromer, B., Neubert, R. E. M., Meijer, H. A. J., Schroeder, H.,  
34 and Levin, I.: Carbon monoxide: A quantitative tracer for fossil fuel CO<sub>2</sub>?, *Journal of*  
35 *Geophysical Research*, 111, 10.1029/2005jd006966, 2006.

36 Geels, C., Gloor, M., Ciais, P., Bousquet, P., Peylin, P., Vermeulen, A. T., Dargaville, R.,  
37 Aalto, T., Brandt, J., Christensen, J. H., Frohn, L. M., Haszpra, L., Karstens, U., Rödenbeck,  
38 C., Ramonet, M., Carboni, G., and Santaguida, R.: Comparing atmospheric transport models  
39 for future regional inversions over Europe &ndash; Part 1: mapping the atmospheric CO<sub>2</sub>  
40 signals, *Atmos. Chem. Phys.*, 7, 3461-3479, 10.5194/acp-7-3461-2007, 2007.

41 Gerbig, C., Körner, S., and Lin, J. C.: Vertical mixing in atmospheric tracer transport models:  
42 error characterization and propagation, *Atmos. Chem. Phys.*, 8, 591-602, 10.5194/acp-8-591-  
43 2008, 2008.

1 Göckede, M., Michalak, A. M., Vickers, D., Turner, D. P., and Law, B. E.: Atmospheric  
2 inverse modeling to constrain regional-scale CO<sub>2</sub> budgets at high spatial and temporal  
3 resolution, *Journal of Geophysical Research: Atmospheres*, 115, D15113,  
4 10.1029/2009JD012257, 2010.

5 Hansen, M. C., and Reed, B.: A comparison of the IGBP DISCover and University of  
6 Maryland 1km global land cover products, *International Journal of Remote Sensing*, 21,  
7 1365-1373, 10.1080/014311600210218, 2000.

8 Hase, F., Frey, M., Blumenstock, T., Groß, J., Kiel, M., Kohlhepp, R., Mengistu Tsidu, G.,  
9 Schäfer, K., Sha, M. K., and Orphal, J.: Application of portable FTIR spectrometers for  
10 detecting greenhouse gas emissions of the major city Berlin, *Atmos. Meas. Tech.*, 8, 3059-  
11 3068, 10.5194/amt-8-3059-2015, 2015.

12 Helfter, C., Famulari, D., Phillips, G. J., Barlow, J. F., Wood, C. R., Grimmond, C. S. B., and  
13 Nemitz, E.: Controls of carbon dioxide concentrations and fluxes above central London,  
14 *Atmos. Chem. Phys.*, 11, 1913-1928, 10.5194/acp-11-1913-2011, 2011.

15 Henne, S., Brunner, D., Oney, B., Leuenberger, M., Eugster, W., Bamberger, I., Meinhardt,  
16 F., Steinbacher, M., and Emmenegger, L.: Validation of the Swiss methane emission  
17 inventory by atmospheric observations and inverse modelling, *Atmos. Chem. Phys.*, 16, 3683-  
18 3710, 10.5194/acp-16-3683-2016, 2016.

19 Hernandez-Paniagua, I. Y., Lowry, D., Clemitshaw, K. C., Fisher, R. E., France, J. L.,  
20 Lanoiselle, M., Ramonet, M., and Nisbet, E. G.: Diurnal, seasonal, and annual trends in  
21 atmospheric CO<sub>2</sub> at southwest London during 2000-2012: Wind sector analysis and  
22 comparison with Mace Head, Ireland, *Atmos. Environ.*, 105, 138-147,  
23 10.1016/j.atmosenv.2015.01.021, 2015.

24 Hogan, R. J., Grant, A. L. M., Illingworth, A. J., Pearson, G. N., and O'Connor, E. J.: Vertical  
25 velocity variance and skewness in clear and cloud-topped boundary layers as revealed by  
26 Doppler lidar, *Quarterly Journal of the Royal Meteorological Society*, 135, 635-643,  
27 10.1002/qj.413, 2009.

28 Jeong, S., Zhao, C., Andrews, A. E., Bianco, L., Wilczak, J. M., and Fischer, M. L.: Seasonal  
29 variation of CH<sub>4</sub> emissions from central California, *Journal of Geophysical Research:*  
30 *Atmospheres*, 117, D11306, 10.1029/2011JD016896, 2012.

31 Kort, E. A., Angevine, W. M., Duren, R., and Miller, C. E.: Surface observations for  
32 monitoring urban fossil fuel CO<sub>2</sub> emissions: minimum site location requirements for the Los  
33 Angeles megacity, *Journal of Geophysical Research: Atmospheres*, n/a-n/a,  
34 10.1002/jgrd.50135, 2013.

35 Kotthaus, S., and Grimmond, C. S. B.: Identification of Micro-scale Anthropogenic CO<sub>2</sub>, heat  
36 and moisture sources - Processing eddy covariance fluxes for a dense urban environment,  
37 *Atmos. Environ.*, 57, 301-316, 10.1016/j.atmosenv.2012.04.024, 2012.

38 Lac, C., Donnelly, R. P., Masson, V., Pal, S., Riette, S., Donier, S., Queguiner, S., Tanguy,  
39 G., Ammoura, L., and Xueref-Remy, I.: CO<sub>2</sub> dispersion modelling over Paris region within  
40 the CO<sub>2</sub>-MEGAPARIS project, *Atmos. Chem. Phys.*, 13, 4941-4961, 10.5194/acp-13-4941-  
41 2013, 2013.

42 Laurent, O., Guemri, A., Yver Kwok, C. E., Rivier, L., Phillippon, C., and Ramonet, M.:  
43 ICOS ATC Metrology Lab: metrological performance assessment of GHG analyzers, 18th

- 1 WMO/IAEA Meeting on Carbon Dioxide, Other Greenhouse Gases, and Related  
2 Measurement Techniques (GGMT-2015), La Jolla, California, September 13-17, 2015, 2015.
- 3 Lauvaux, T., Schuh, A. E., Uliasz, M., Richardson, S., Miles, N., Andrews, A. E., Sweeney,  
4 C., Diaz, L. I., Martins, D., Shepson, P. B., and Davis, K. J.: Constraining the  
5 CO<sub>2</sub> budget of the corn belt: exploring uncertainties from the assumptions in a  
6 mesoscale inverse system, *Atmos. Chem. Phys.*, 12, 337-354, 10.5194/acp-12-337-2012,  
7 2012.
- 8 Levin, I., Hammer, S., Eichelmann, E., and Vogel, F. R.: Verification of greenhouse gas  
9 emission reductions: the prospect of atmospheric monitoring in polluted areas, *Philosophical*  
10 *Transactions of the Royal Society A: Mathematical, Physical and*  
11 *Engineering Sciences*, 369, 1906-1924, 10.1098/rsta.2010.0249, 2011.
- 12 Lowry, D., Holmes, C. W., Rata, N. D., O'Brien, P., and Nisbet, E. G.: London methane  
13 emissions: Use of diurnal changes in concentration and  $\delta^{13}\text{C}$  to identify urban sources and  
14 verify inventories, *Journal of Geophysical Research*, 106, 7427, 10.1029/2000jd900601,  
15 2001.
- 16 MACC-II: [www.copernicus-atmosphere.eu](http://www.copernicus-atmosphere.eu), access: 01/09/2012, 2012.
- 17 Masuda, S., Suzuki, S., Sano, I., Li, Y.-Y., and Nishimura, O.: The seasonal variation of  
18 emission of greenhouse gases from a full-scale sewage treatment plant, *Chemosphere*, 140,  
19 167-173, <http://dx.doi.org/10.1016/j.chemosphere.2014.09.042>, 2015.
- 20 Masutani, M., Schlatter, T. W., Errico, R. M., Stoffelen, A., Andersson, E., Lahoz, W.,  
21 Woollen, J. S., Emmitt, G. D., Riishøjgaard, L.-P., Lord, S. J.: Observing system simulation  
22 experiments, in: *Data Assimilation: Making Sense of Observations*, edited by: Lahoz, W. A.,  
23 Khatatov, B., Ménard, R., Springer, Berlin, 647-679, 2010.
- 24 McKain, K., Wofsy, S. C., Nehrkorn, T., Eluszkiewicz, J., Ehleringer, J. R., and Stephens, B.  
25 B.: Assessment of ground-based atmospheric observations for verification of greenhouse gas  
26 emissions from an urban region, *Proc. Natl. Acad. Sci. U. S. A.*, 109, 8423-8428,  
27 10.1073/pnas.1116645109, 2012.
- 28 McKain, K. K., Down, A., Raciti, S. M., Budney, J., Hutyra, L. R., Floerchinger, C.,  
29 Herndon, S. C., Nehrkorn, T., Zahniser, M. S., Jackson, R. B., Phillips, N., and Wofsy, S. C.:  
30 Methane emissions from natural gas infrastructure and use in the urban region of Boston,  
31 Massachusetts, *Proc. Natl. Acad. Sci. U. S. A.*, 112, 1941-1946, 10.1073/pnas.1416261112,  
32 2015.
- 33 National Atmospheric Emissions Inventory: <http://naei.defra.gov.uk/>, access: 12/12/2013,  
34 2013.
- 35 Nakagawa, F., Tsunogai, U., Komatsu, D. D., Yamada, K., Yoshida, N., Moriizumi, J.,  
36 Nagamine, K., Iida, T., and Ikebe, Y.: Automobile exhaust as a source of C-13- and D-  
37 enriched atmospheric methane in urban areas, *Org Geochem*, 36, 727-738,  
38 10.1016/j.orggeochem.2005.01.003, 2005.
- 39 Nehrkorn, T., Henderson, J., Leidner, M., Mountain, M., Eluszkiewicz, J., McKain, K., and  
40 Wofsy, S.: WRF Simulations of the Urban Circulation in the Salt Lake City Area for CO<sub>2</sub>  
41 Modeling, *Journal of Applied Meteorology and Climatology*, 52, 323-340, 10.1175/JAMC-D-  
42 12-061.1, 2013.
- 43 Newman, S., Jeong, S., Fischer, M. L., Xu, X., Haman, C. L., Lefer, B., Alvarez, S.,  
44 Rappenglueck, B., Kort, E. A., Andrews, A. E., Peischl, J., Gurney, K. R., Miller, C. E., and

1 Yung, Y. L.: Diurnal tracking of anthropogenic CO<sub>2</sub> emissions in the Los Angeles basin  
2 megacity during spring 2010, *Atmos. Chem. Phys.*, 13, 4359-4372, 10.5194/acp-13-4359-  
3 2013, 2013.

4 NOAA Mace Head Atmospheric Station Data:  
5 <http://www.esrl.noaa.gov/gmd/dv/data/?site=MHD>, access: 23/01/2014, 2013.

6 Nordbo, A., Järvi, L., Haapanala, S., Wood, C. R., and Vesala, T.: Fraction of natural area as  
7 main predictor of net CO<sub>2</sub> emissions from cities, *Geophys. Res. Lett.*, 39,  
8 10.1029/2012gl053087, 2012.

9 O'Shea, S. J., Allen, G., Fleming, Z. L., Bauguitte, S. J. B., Percival, C. J., Gallagher, M. W.,  
10 Lee, J., Helfter, C., and Nemitz, E.: Area fluxes of carbon dioxide, methane, and carbon  
11 monoxide derived from airborne measurements around Greater London: A case study during  
12 summer 2012, *Journal of Geophysical Research: Atmospheres*, 119, 2013JD021269,  
13 10.1002/2013JD021269, 2014.

14 Pregger, T., and Friedrich, R.: Effective pollutant emission heights for atmospheric transport  
15 modelling based on real-world information, *Environ. Pollut.*, 157, 552-560,  
16 10.1016/j.envpol.2008.09.027, 2009.

17 Reis, S., Lang, M., and Vieno, M.: Improving the temporal profiles of emission input data for  
18 high resolution atmospheric transport modeling-a case study for the UK. , 18th Annual  
19 International Emission Inventory Conference, Baltimore, USA., 2009,

20 Rella, C. W., Chen, H., Andrews, A. E., Filges, A., Gerbig, C., Hatakka, J., Karion, A., Miles,  
21 N. L., Richardson, S. J., Steinbacher, M., Sweeney, C., Wastine, B., and Zellweger, C.: High  
22 accuracy measurements of dry mole fractions of carbon dioxide and methane in humid air,  
23 *Atmos. Meas. Tech.*, 6, 837-860, 10.5194/amt-6-837-2013, 2013.

24 Rigby, M., Toumi, R., Fisher, R., Lowry, D., and Nisbet, E. G.: First continuous  
25 measurements of CO<sub>2</sub> mixing ratio in central London using a compact diffusion probe,  
26 *Atmos. Environ.*, 42, 8943-8953, 10.1016/j.atmosenv.2008.06.040, 2008.

27 Schmidt, H., Derognat, C., Vautard, R., and Beekmann, M.: A comparison of simulated and  
28 observed ozone mixing ratios for the summer of 1998 in Western Europe, *Atmos. Environ.*,  
29 35, 6277-6297, 10.1016/s1352-2310(01)00451-4, 2001.

30 Stauer, J., Broquet, G., Bréon, F. M., Puygrenier, V., Chevallier, F., Xueref-Rémy, I.,  
31 Dieudonné, E., Lopez, M., Schmidt, M., Ramonet, M., Perrussel, O., Lac, C., Wu, L., and  
32 Ciais, P.: A first year-long estimate of the Paris region fossil fuel CO<sub>2</sub> emissions based on  
33 atmospheric inversion, *Atmos. Chem. Phys. Discuss.*, 2016, 1-34, 10.5194/acp-2016-191,  
34 2016.

35 Townsend-Small, A., Tyler, S. C., Pataki, D. E., Xu, X., and Christensen, L. E.: Isotopic  
36 measurements of atmospheric methane in Los Angeles, California, USA: Influence of  
37 "fugitive" fossil fuel emissions, *Journal of Geophysical Research*, 117,  
38 10.1029/2011jd016826, 2012.

39 Turnbull, J. C., Sweeney, C., Karion, A., Newberger, T., Lehman, S. J., Tans, P. P., Davis, K.  
40 J., Lauvaux, T., Miles, N. L., Richardson, S. J., Cambaliza, M. O., Shepson, P. B., Gurney,  
41 K., Patarasuk, R., and Razlivanov, I.: Toward quantification and source sector identification  
42 of fossil fuel CO<sub>2</sub> emissions from an urban area: Results from the INFLUX experiment,  
43 *Journal of Geophysical Research: Atmospheres*, 120, 2014JD022555,  
44 10.1002/2014JD022555, 2015.

1 Met Office Integrated Data Archive System (MIDAS) Land and Marine Surface Stations Data  
2 (1853-current): [http://badc.nerc.ac.uk/view/badc.nerc.ac.uk\\_ATOM\\_dataent\\_ukmo-midas](http://badc.nerc.ac.uk/view/badc.nerc.ac.uk_ATOM_dataent_ukmo-midas)  
3 access: 29/09/2013, 2012.

4 United Nations: World Population Prospects: 2011 Revision 2012.

5 Vogel, F. R., Hammer, S., Steinhof, A., Kromer, B., and Levin, I.: Implication of weekly and  
6 diurnal <sup>14</sup>C calibration on hourly estimates of CO<sub>2</sub>-based fossil fuel CO<sub>2</sub> at a moderately  
7 polluted site in southwestern Germany, *Tellus B*, 62, 512-520, 10.1111/j.1600-  
8 0889.2010.00477.x, 2010.

9 Ward, H. C., Kotthaus, S., Grimmond, C. S. B., Bjarkegren, A., Wilkinson, M., Morrison, W.  
10 T. J., Evans, J. G., Morrison, J. I. L., and Iamarino, M.: Effects of urban density on carbon  
11 dioxide exchanges: Observations of dense urban, suburban and woodland areas of southern  
12 England, *Environ. Pollut.*, 198, 186-200, <http://dx.doi.org/10.1016/j.envpol.2014.12.031>,  
13 2015.

14 GAW Report No. 206:  
15 [http://www.wmo.int/pages/prog/arep/gaw/documents/Final\\_GAW\\_206\\_web.pdf](http://www.wmo.int/pages/prog/arep/gaw/documents/Final_GAW_206_web.pdf), 2012.

16 Wu, L., Broquet, G., Ciais, P., Bellassen, V., Vogel, F., Chevallier, F., Xueref-Remy, I., and  
17 Wang, Y.: Atmospheric inversion for cost effective quantification of city CO<sub>2</sub>  
18 emissions, *Atmos. Chem. Phys. Discuss.*, 2015, 30693-30756, 10.5194/acpd-15-30693-2015,  
19 2015.

20 Wunch, D., Wennberg, P. O., Toon, G. C., Keppel-Aleks, G., and Yavin, Y. G.: Emissions of  
21 greenhouse gases from a North American megacity, *Geophys. Res. Lett.*, 36,  
22 10.1029/2009gl039825, 2009.

23 Yver Kwok, C. E., Müller, D., Caldow, C., Lebègue, B., Mønster, J. G., Rella, C. W.,  
24 Scheutz, C., Schmidt, M., Ramonet, M., Warneke, T., Broquet, G., and Ciais, P.: Methane  
25 emission estimates using chamber and tracer release experiments for a municipal waste water  
26 treatment plant, *Atmos. Meas. Tech.*, 8, 2853-2867, 10.5194/amt-8-2853-2015, 2015.

27 Zellweger, C., Steinbacher, M., and Buchmann, B.: Evaluation of new laser spectrometer  
28 techniques for in-situ carbon monoxide measurements, *Atmos. Meas. Tech.*, 5, 2555-2567,  
29 10.5194/amt-5-2555-2012, 2012.

30  
31

1 Table 1: Summary of systematic and random errors of hourly measurements (see Sect. 2.3)  
 2 and of the hourly model–data discrepancies using data between 12:00 and 17:00 during July  
 3 to September 2012. Values are given for CO<sub>2</sub> (CH<sub>4</sub> in brackets) in parts per million (ppm) and  
 4 parts per billion (ppb) for CH<sub>4</sub>. STD denotes standard deviation; RMS denotes root mean  
 5 square.  
 6

Error Type	Measurement error	Model–data discrepancies			
		Detling	Hackney	Poplar	Teddington
Bias	STD of bias: 1.0 (5)	−5.3 (−19.0)	−9.1 (−20.7)	−5.5 (−28.6)	−5.7 (−13.3)
STD	0.3 (8)	6.5 (27.4)	7.3 (43.2)	7.1 (46.9)	7.1 (29.3)
RMS	-	8.4 (33.3)	11.7 (47.9)	9.0 (54.9)	9.1 (32.2)

1 Table 2: Summary of systematic and random errors of hourly measured gradients (see Sect.  
2 3.5, the standard deviation of the measurement error for gradients is computed as  $\sqrt{2}$  times the  
3 value of Table 1, assuming null correlation of this error between different sites) and of the  
4 hourly gradient model–data discrepancies using data between 12:00 and 17:00 during July to  
5 September 2012. Values are given for  $\Delta\text{CO}_2$  ( $\Delta\text{CH}_4$  in brackets) in parts per million (ppm)  
6 and parts per billion (ppb) for  $\text{CH}_4$ . The two last columns present discrepancies for afternoon  
7 gradients to Teddington wherein Heathrow measured wind direction places Teddington  
8 upwind of each urban site (for angles between the wind direction and the direction between  
9 Teddington and a given urban site smaller than  $20^\circ$ , see Sect. 3.6). STD denotes standard  
10 deviation; RMS denotes root mean square.

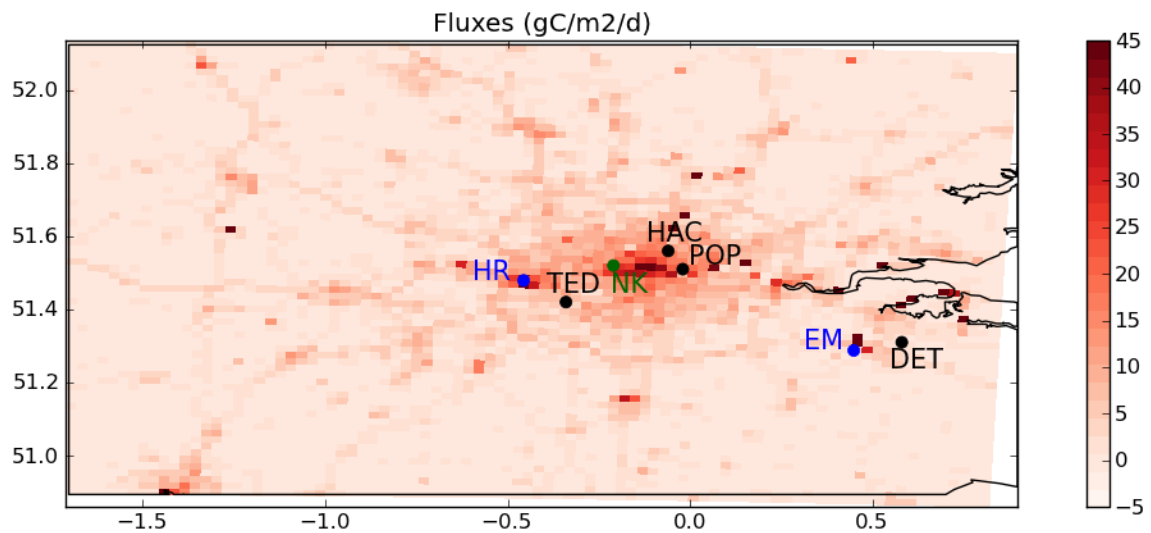
	Gradient measurement error	All afternoon discrepancies				Teddington upwind discrepancies only	
		HAC–DET	POP–DET	HAC–TED	POP–TED	HAC–TED	POP–TED
Bias	STD of bias: 0.0 (0)	–3.8 (–2.6)	–0.2 (–9.7)	–2.9 (–7.1)	0.6 (–16.1)	–1.4 (–3.5)	1.7 (–10.8)
STD	0.4 (11)	5.1 (34.4)	4.4 (36.6)	4.2 (28.3)	3.6 (32.2)	2.9 (14.5)	3.4 (11.0)
RMS	-	6.3 (34.4)	5.1 (29.2)	4.4 (37.8)	3.6 (36.0)	3.2 (14.8)	3.7 (15.3)

11  
12  
13

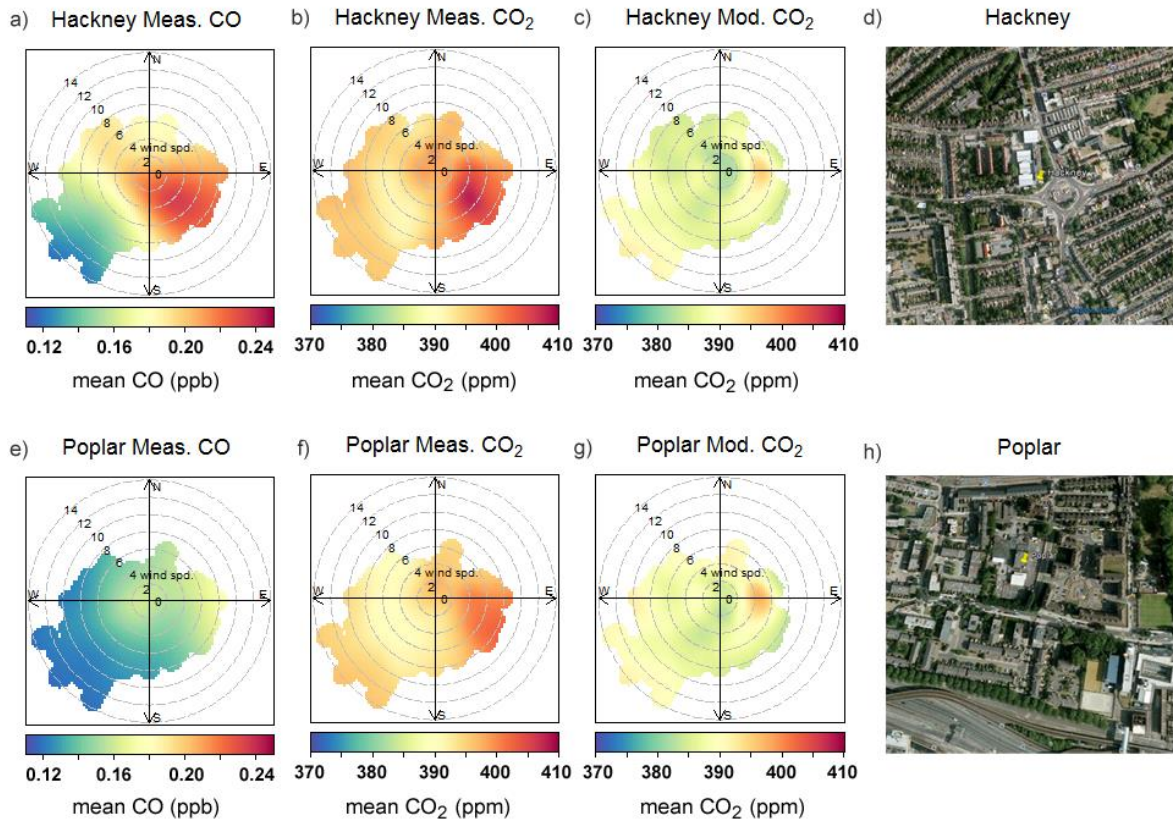
1 Table 3: Statistics of the hourly difference between modelled and observationally based fossil  
 2 fuel CO<sub>2</sub> gradients ( $\Delta\text{FF-CO}_2$ ) in parts per million (ppm) for HAC–TED and POP–TED  
 3 during the afternoon periods (12:00 to 17:00) between July and September, when Heathrow  
 4 measured wind direction places Teddington upwind of each urban site (for angles between the  
 5 wind direction and the direction between Teddington and a given urban site smaller than 20°,  
 6 see Sect. 3.6). RMS denotes root mean square.

Error Type	HAC–TED	POP–TED
Bias	–0.4	2.8
RMS	2.5	3.6



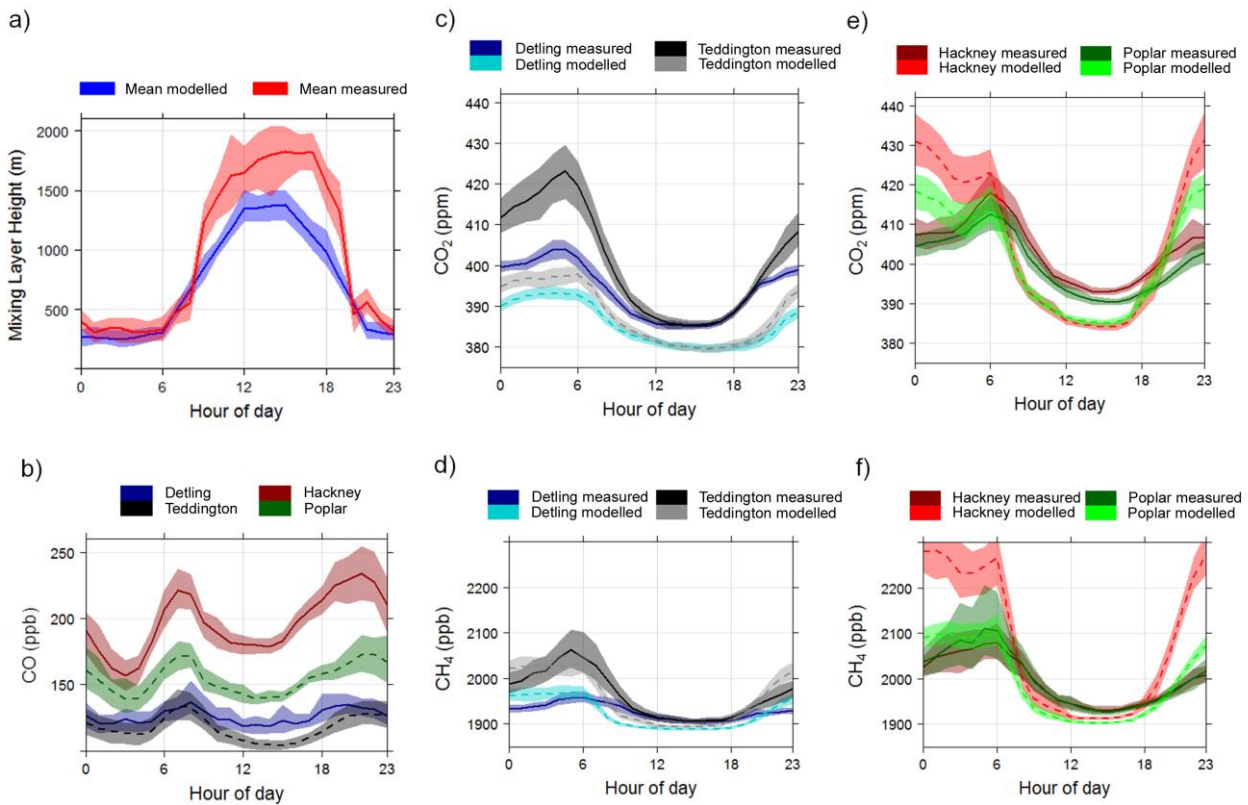


1  
 2 Figure 1: Map of the spatially derived (at 2-km resolution) CO<sub>2</sub> fossil fuel emissions  
 3 inventories (gC m<sup>-2</sup> d<sup>-1</sup>) for the London section of the model domain, indicating the location  
 4 of the four GHG measurement stations (black), the two meteorological sites Heathrow (HR)  
 5 and East Malling (EM) (blue) and the North Kensington LIDAR site (NK, green). Dark red  
 6 corresponds to relatively high CO<sub>2</sub> values (45 gC m<sup>-2</sup> d<sup>-1</sup>) and light pink to relatively low  
 7 CO<sub>2</sub> values (-5 gC m<sup>-2</sup> d<sup>-1</sup>).  
 8

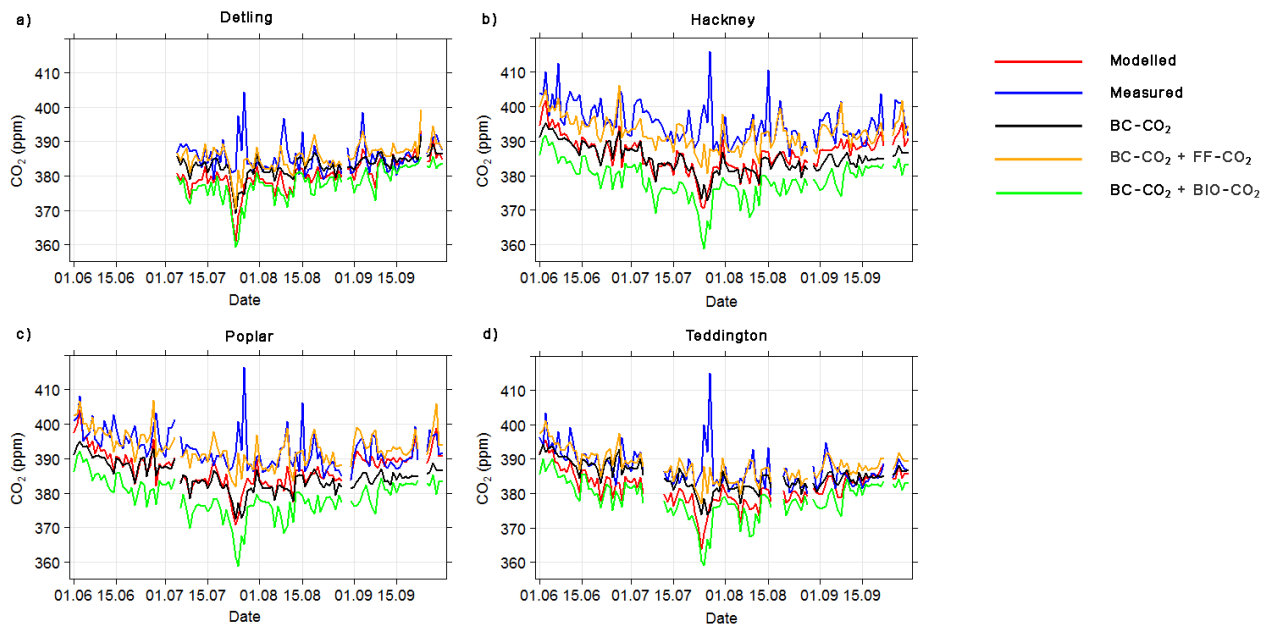


1  
 2 Figure 2: Wind roses for each urban measurement site incorporating hourly data for wind  
 3 speed, wind direction (Heathrow measured data) and CO<sub>2</sub> mole fraction between the hours  
 4 12:00 and 17:00 for a) observed CO mole fractions at Hackney, b) observed CO<sub>2</sub> mole  
 5 fractions at Hackney, c) modelled CO<sub>2</sub> mole fractions at Hackney, d) a map (© 2012 Google-  
 6 Imagery and Bluesky, the GeoInformation group) of the immediate vicinity of the Hackney  
 7 site, e) observed CO mole fractions at Poplar, f) observed CO<sub>2</sub> mole fractions at Poplar, g)  
 8 modelled CO<sub>2</sub> mole fractions at Poplar and h) a map (© 2012 Google-Imagery and Bluesky,  
 9 the GeoInformation group) of the immediate vicinity of the Poplar site. The colours on the  
 10 wind roses show the gas mole fraction (parts per million, ppm) with the radius corresponding  
 11 to the magnitude of the windspeed ( $\text{m s}^{-1}$ ) and the azimuthal angle to the wind direction ( $^{\circ}\text{N}$ ).  
 12 Red corresponds to relatively high concentrations and blue to relatively low concentrations  
 13 within the given scale of each gas (min = 0.11 parts per billion (ppb) and max = 0.25 ppb for  
 14 CO, and min = 370 ppm, max = 410 ppm for CO<sub>2</sub>).

15



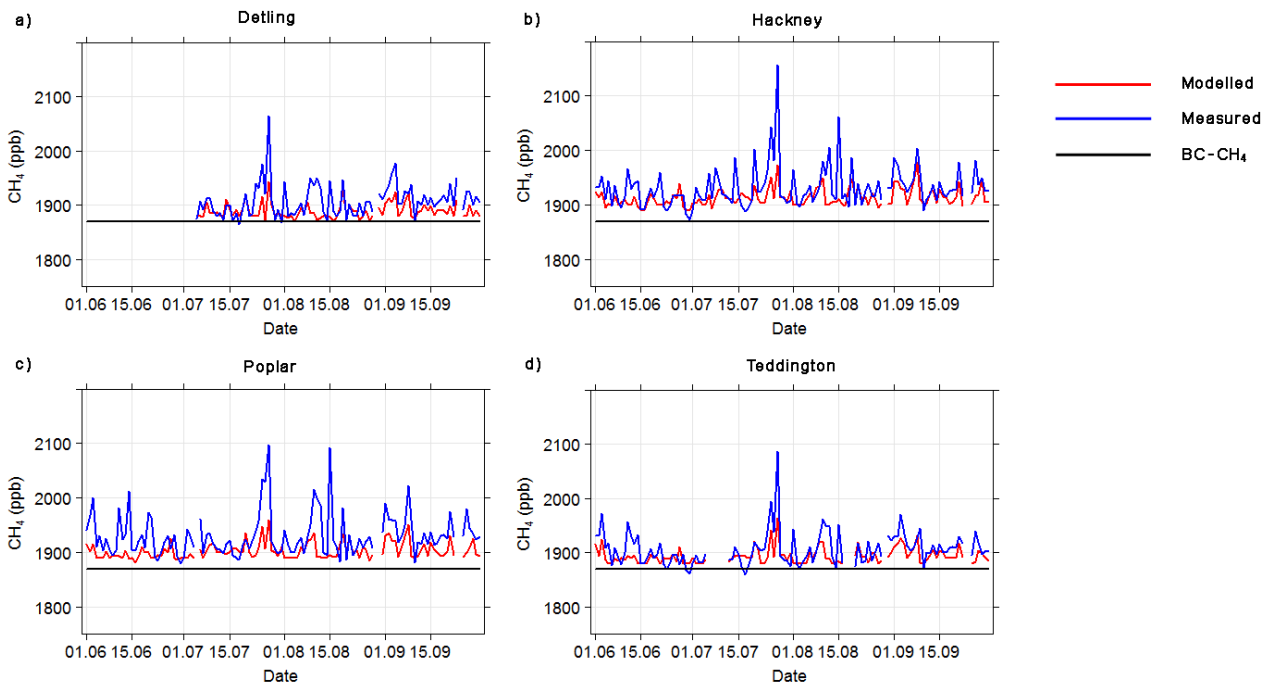
1  
 2 Figure 3: Mean diurnal cycles of a) modelled (blue) and measured (red) boundary layer height  
 3 and measured mean mixing layer height at North Kensington based on the spectral correction  
 4 method described in Sect. 2.5, b) measured CO mole fractions at the rural (Detling, blue),  
 5 suburban (Teddington, black), and urban sites (Hackney, red and Poplar, green), c) modelled  
 6 (light shade) and measured (dark shade) CO<sub>2</sub> mole fractions at the rural (Detling, blue) and  
 7 suburban (Teddington, black) sites, d) modelled and measured (dark shade) CH<sub>4</sub> mole  
 8 fractions at the rural (Detling, blue) and suburban (Teddington, black) sites d) modelled (light  
 9 shade) and measured (dark shade) CO<sub>2</sub> mole fractions at the urban (Hackney, red and Poplar,  
 10 green) sites and f) modelled and measured CH<sub>4</sub> mole fractions at the urban (Hackney, red and  
 11 Poplar, green) sites. June data are excluded due to unavailability of data during this period at  
 12 Detling. Shading represents an estimate of the 95% confidence interval in the mean, related to  
 13 the limitation of the sampling of the daily values at a given hour (based on the division of two  
 14 times their temporal standard deviation by the square root of the number of values).  
 15



1

2 Figure 4: Time series of averages for the afternoon period (12:00 to 17:00) each day of  
 3 modelled CO<sub>2</sub> mole fractions (red), measured CO<sub>2</sub> mole fractions (blue), modelled signature  
 4 of the CO<sub>2</sub> boundary condition mole fractions from MACC-II (BC-CO<sub>2</sub>, black), the modelled  
 5 signature of the CO<sub>2</sub> fossil fuel emissions added to that of the boundary conditions (BC-CO<sub>2</sub>  
 6 + FF-CO<sub>2</sub>, orange) and the modelled signature of the CO<sub>2</sub> NEE added to that of the boundary  
 7 conditions (BC-CO<sub>2</sub> + BIO-CO<sub>2</sub>, green) at a) Detling, b) Hackney, c) Poplar and d)  
 8 Teddington.

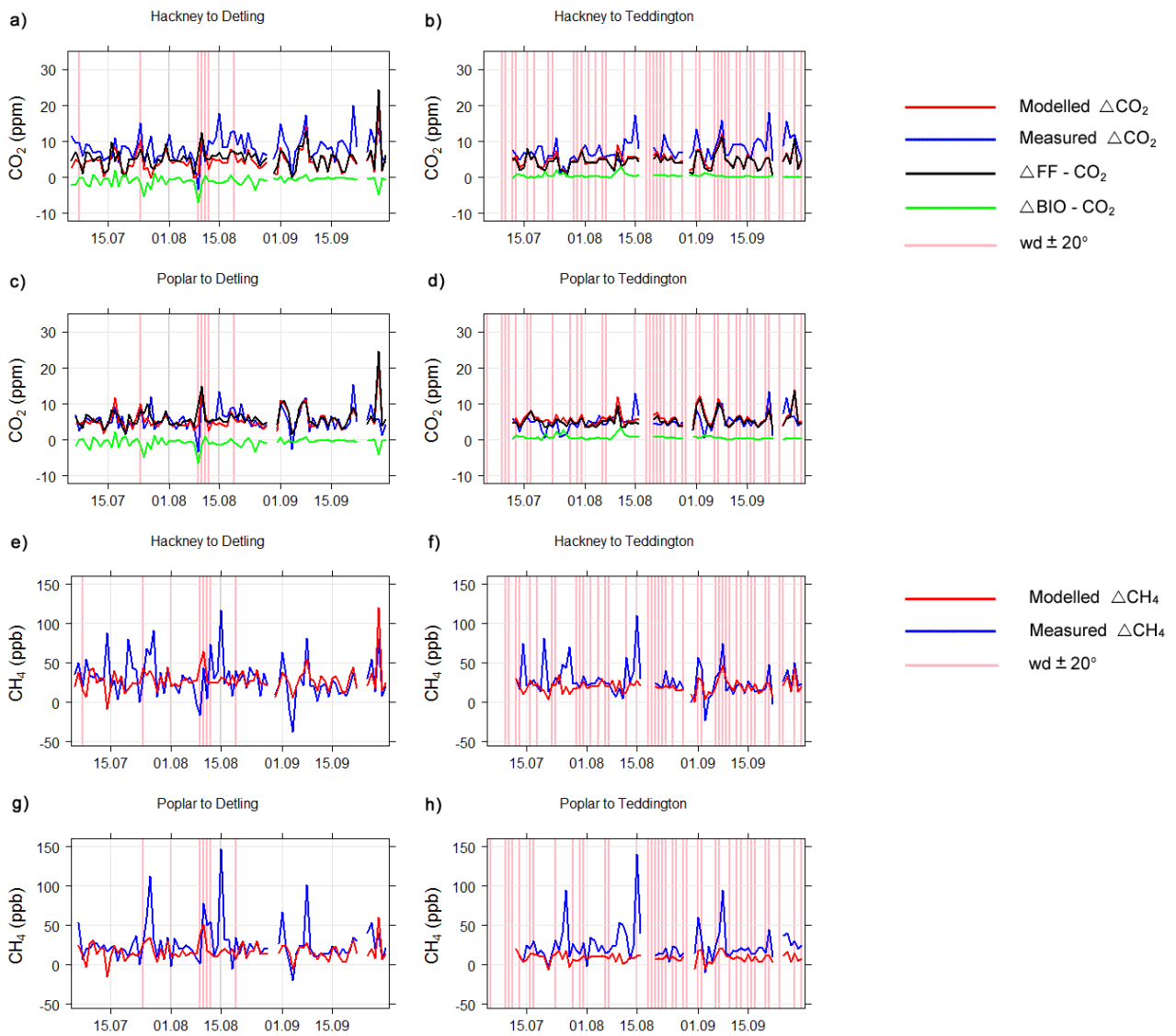
9



1

2 Figure 5: Time series of averages for the afternoon period (12:00 to 17:00) each day of  
 3 measured CH<sub>4</sub> mole fractions (blue), modelled CH<sub>4</sub> mole fractions (red) and the constant  
 4 signature of the modelled CH<sub>4</sub> boundary conditions (BC-CH<sub>4</sub>, black) at a) Detling, b)  
 5 Hackney, c) Poplar and d) Teddington.

6



1  
 2 Figure 6: Time series of averages for the afternoon period (12:00 to 17:00) each day of  
 3 measured  $\Delta\text{CO}_2$  (blue), modelled  $\Delta\text{CO}_2$  (red), modelled signature of the fossil fuel  $\text{CO}_2$   
 4 emissions ( $\Delta\text{FF-CO}_2$ ) (black) and modelled signature of the  $\text{CO}_2$  NEE ( $\Delta\text{BIO-CO}_2$ ) (green)  
 5 between a) Hackney and Detling, b) Hackney and Teddington, c) Poplar and Detling and d)  
 6 Poplar and Teddington. Time series of averages for the afternoon period (12:00 to 17:00) of  
 7 measured (dark and light blue) or measured (red and orange)  $\Delta\text{CH}_4$  between e) Hackney or f)  
 8 Poplar and Detling (dark blue and red) or g) Hackney and h) Poplar and Teddington (light  
 9 blue or orange). Vertical pink lines indicate days during which at least one hourly afternoon  
 10 wind direction is within a  $\pm 20^\circ$  range around the direction from the reference site to the urban  
 11 site according to the wind measurements at Heathrow (if the reference site is Teddington) or  
 12 East Malling (if the reference site is Detling).